JCI The Journal of Clinical Investigation

Humanized neurofibroma model from induced pluripotent stem cells delineates tumor pathogenesis and developmental origins

Juan Mo, … , David H. Gutmann, Lu Q. Le

J Clin Invest. 2020. https://doi.org/10.1172/JCI139807.

Research In-Press Preview **Neuroscience** **Oncology**

Graphical abstract

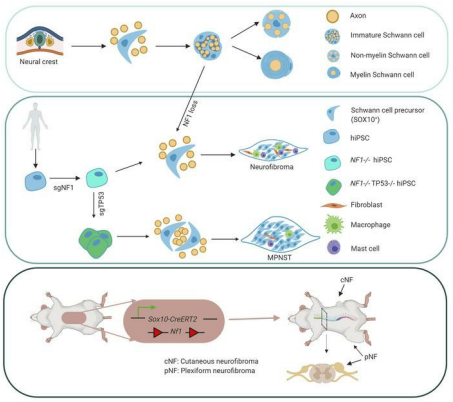

Humanized Neurofibroma Model from Induced Pluripotent Stem Cells Delineates Tumor Pathogenesis and Developmental Origins

Juan Mo[1], Corina Anastasaki[2], Zhiguo Chen[1], Tracey Shipman[1], Jason Papke[2], Kevin Yin[1], David H. Gutmann[2,5], Lu Q. Le[1,3,4,5]

[1]Department of Dermatology, UT Southwestern Medical Center, Dallas, TX, USA
[2]Department of Neurology, Washington University School of Medicine, St. Louis, MO, USA
[3]Simmons Comprehensive Cancer Center, UT Southwestern Medical Center, Dallas, TX, USA
[4]Hamon Center for Regenerative Science and Medicine, UT Southwestern Medical Center, Dallas, TX, USA

[5]Corresponding authors:

Lu Q. Le, M.D., Ph.D.
Professor
Department of Dermatology
Simmons Comprehensive Cancer Center
Hamon Center for Regenerative Science and Medicine
UT Southwestern Medical Center
Dallas, TX 75248
Phone: (214) 648-5781
Fax: (214) 648-5553
E-mail: Lu.Le@UTSouthwestern.edu

David H. Gutmann, M.D., Ph.D.
Professor
Department of Neurology
Washington University School of Medicine
St. Louis, MO 63110
Phone: (314) 362-7379
Fax: (314) 362-2388
E-mail: gutmannd@wustl.edu

Running title: Humanized Neurofibromas Reveal Tumor Pathogenesis & Origin

Conflict of interest: The authors have declared that no conflict of interest exists.

Keywords
Human iPSC, Neurofibromatosis type 1 (NF1), plexiform neurofibroma (pNF), cutaneous neurofibroma (cNF), Schwann cell precursors (SCP), SOX10, malignant peripheral nerve sheath tumor (MPNST)

Abstract

Neurofibromatosis type 1 (NF1) is a common tumor predisposition syndrome, caused by *NF1* gene mutation, in which affected patients develop Schwann cell lineage peripheral nerve sheath tumors (neurofibromas). To investigate human neurofibroma pathogenesis, we differentiated a series of isogenic patient-specific *NF1*-mutant human induced-pluripotent stem cells (hiPSCs) into Schwannian lineage cells (SLCs). We found that while wild-type and heterozygous *NF1*-mutant hiPSC-SLCs did not form tumors following mouse sciatic nerve implantation, *NF1*-null SLCs formed bona fide neurofibromas with high levels of SOX10 expression. To confirm that $SOX10^+$ SLCs contain the cells of origin for neurofibromas, both *Nf1* alleles were inactivated in mouse $Sox10^+$ cells, leading to classic nodular cutaneous and plexiform neurofibroma formation that completely recapitulate their human counterparts. Moreover, we discovered that *NF1* loss impaired Schwann cell differentiation by inducing a persistent stem-like state to expand the pool of progenitors required to initiate tumor formation, indicating that in addition to regulating MAPK-mediated cell growth, *NF1* loss also alters Schwann cell differentiation to promote neurofibroma development. Taken together, we established complementary humanized neurofibroma explant and first-in-kind mouse genetically engineered nodular cutaneous neurofibroma models that delineate neurofibroma pathogenesis amenable to future therapeutic target discovery and evaluation.

Introduction

Neurofibromatosis type 1 (NF1), caused by germline mutations in the *NF1* gene, is one of the most common human genetic disorders affecting the nervous system. As such, individuals with NF1 are prone to the development of multiple central and peripheral nervous system tumors. While gliomas predominate in the central nervous system, children and adults are prone to the formation of two major types of peripheral nerve sheath tumors (neurofibromas): (1) plexiform neurofibromas (pNFs) and (2) dermal or cutaneous neurofibromas (cNFs). pNFs typically involve multiple nerves or a nerve plexus, are congenital in origin, disfiguring, associated with abnormal bone growth or erosion, and harbor a lifelong risk of malignant transformation into deadly malignant peripheral nerve sheath tumors (MPNSTs). In contrast, cNFs usually begin to appear in late childhood and early adolescence and continue to increase in size and number throughout life, often numbering in the thousands in some adults.

Previous studies using genetically engineered murine models have revealed that neurofibromas most likely derive from Schwannian lineage cells (SLCs) following somatic loss of the remaining *Nf1* allele (1-7). While bi-allelic *Nf1* inactivation in early Schwann cell precursors (SCPs) is an obligate step in murine tumorigenesis, there is also a role for the tumor microenvironment in promoting and facilitating neurofibroma formation and progression (8-11). The interplay between impaired NF1 protein (neurofibromin) inhibition of MEK/ERK-mediated SCP growth and mitogenic signals from non-neoplastic stromal cells has facilitated the identification of novel treatments for plexiform neurofibromas (10, 12-14). Unfortunately, there are no equivalent murine models of discrete cutaneous neurofibroma and no accurate humanized *in vivo* neurofibroma models.

To address this critical barrier, we employed a unique series of human induced-pluripotent stem cells (hiPSCs) harboring NF1 patient *NF1* gene mutations to generate proliferating SCPs and examine the impact of *NF1* mutation on Schwann cell lineage differentiation, as well as generate human neurofibromas in mice. Using this approach,

we found that *NF1* loss delays SLC differentiation by expanding the pool of progenitors necessary to initiate tumor formation. Moreover, we successfully generated humanized neurofibroma and MPNST models in mice that faithfully phenocopy the analogous tumors in patients. Lastly, we leveraged this humanized experimental system to identify a subpopulation of $SOX10^{+}$ SCPs, which we exploited to establish the first genetically engineered mouse model of nodular/discrete cNF. Taken together, these human-derived neurofibroma and MPNST models have the potential to serve as tractable platforms for drug identification and screening, as well as to provide unprecedented opportunities to elucidate the mechanisms underlying neurofibroma development and progression.

Results

Differentiation of Patient-Derived Isogenic hiPSCs Directly into Schwann Cell Precursors

Schwann cell precursors (SCPs) have previously been shown to contain the cells of origin for plexiform neurofibroma (4). These progenitors represent intermediate and multipotent stage neural crest-derived cells that emerge following neural tube closure during early embryonic development (15). SCPs provide essential survival signals for developing neurons (16), and guide multipotent cells to specific cell fates and locations (17). In rodents, SCPs are found in the dorsal root ganglion (DRG) (mouse, E12-14; rat, E14-15) (4, 18, 19), where they contribute to the generation of immature Schwann cells (iSCs), which later diversify into non-myelinating (Remak) and myelinating Schwann cells.

For this reason, we differentiated patient-derived isogenic hiPSCs (20) directly into SCPs using DMEM/F12-Neural Basal-N2B27 media supplemented with SB431542 (Activin and TGF-β inhibitor to prevent SMAD signaling, suppress pluripotency, and prevent mesoderm/endoderm induction), a GSK3 inhibitor (CHIR99021; to activate WNT signaling), and higher concentrations of neuregulin β-1 to support glial fate differentiation (21). Before differentiation, the cells formed colonies **(Figure 1A and Supplemental Figure 1A)**, which are characteristic of hiPSCs and were immunopositive for pluripotent

markers, including NANOG, SOX2, Oct3/4, and TRA1-60 **(Figure 1A)**. The pluripotency of these hiPSCs was also confirmed by teratoma formation **(Supplemental Figure 1B)**. Following differentiation, the typical SCP cell shape (elongated bipolar or tripolar dendrites) was distinct from that of hiPSCs (**Figure 1**). The successful differentiation of hiPSCs into SCPs was confirmed by decreased Oct3/4 and NANOG expression (**Figure 1B and Supplemental Figure 2A-B**) and increased expression of SCP markers, including SOX10, HOXb7, GAP43, AP2a (**Figure 1B-C**), and p75 protein (**Figure 1B, Figure 2A-C**) and *MPZ*, *CDH19*, *ITGA4*, and *PLP* mRNA (**Figure 2D**). The adult neural stem cell marker, Nestin, was also expressed in these hiPSC-derived SCPs cells (hiPSC-SCPs) (**Figure 1C**). SOX10 and AP2a contribute to the gene regulatory network required for neural crest formation during the emigration of the neural crest progenitors from the neural tube through an epithelial to mesenchymal transition (EMT). The co-localization of SOX10 and HOXb7 in hiPSC-SCPs (**Figure 1B**) suggests that the SOX10-expressing cell population also contains HOXb7-expressing cells, which we previously identified to contain the cells of origin for plexiform and cutaneous neurofibroma in mice (6).

To determine whether these cells are proliferating, we incubated the cells with BrdU and then co-stained for markers of SCPs: AP2a, SOX10, and HOXb7. (**Supplemental Figure 1C**). We observed co-localization of these SCP markers with BrdU, indicating that these cells are proliferating, with quantification showing that *NF1-/-* hiPSC-SCPs had the highest numbers of proliferating cells (**Supplemental Figure 1D-F**).

NF1 Loss Impairs Schwann Cell Lineage Differentiation

Since neurofibromin functions as a negative growth regulator through its ability to accelerate the conversion of active GTP-bound RAS to inactive GDP-bound RAS, loss of *NF1* results in RAS pathway activation, leading to aberrant growth of SLC cells and the formation of neurofibromas (22, 23). In addition, neurofibromin also regulates differentiation and proliferation of several nervous system cell types, including neural stem cells and neuroglial progenitors *in vitro* and *in vivo* in cell type-, cell function-, and brain region-specific manners (24, 25).

To evaluate the role of the *NF1* gene in SLC differentiation, we examined isogenic *NF1*$^{+/+}$ (WT isogenic control), *NF1*$^{+/-}$ (heterozygous patient-derived *NF1* mutation) and *NF1*$^{-/-}$ (homozygous patient-derived *NF1* mutation) hiPSCs. First, following differentiation, we observed decreased expression of the *Oct3/4* and *NANOG* pluripotent markers **(Supplemental Figure 2A-B**). In addition, the percentage of p75-expressing cells (SCPs) among the isogenic lines decreased from 90.4% in *NF1*$^{+/+}$ hiPSC-SCPs to 81.1% and 62.5% in *NF1*$^{+/-}$ and *NF1*$^{-/-}$ hiPSC-SCPs, respectively (**Figure 2A-C**). Second, we found that *NF1*$^{-/-}$ hiPSC-SCPs had lower (2 to 8-fold change) mRNA levels of SLC markers, including *MPZ*, *CDH19*, *PLP*, *SOX10*, and *ITGA4A* (**Figure 2D**). Third, differentiated *NF1*$^{-/-}$ hiPSC-SCPs expressed higher mRNA (2 to 10-fold change) levels of NCSC markers (*TWIST*, *SLUG* and *SNAIL*) (**Supplemental Figure 2C-E**) relative to their control *NF1*$^{+/+}$ counterparts. Fourth, when hiPSC-SCPs were evaluated for the percentage or frequency of cells that could form self-renewing and multipotent neurospheres (26), *NF1*$^{-/-}$ hiPSC-SCPs neurospheres had 11.84% larger average diameters, 58.82% greater numbers of neurospheres per well, and 84.61% higher frequencies of neurosphere formation relative to *NF1*$^{+/+}$ hiPSC-SCPs **(Figure 2E-G)**. Taken together, these findings suggest that *NF1* loss increases the number of SLC stem cells (Schwann cell precursors, SCPs) (19).

Next, we evaluated the effect of *NF1* loss on SCP proliferation. While *NF1*$^{-/-}$ hiPSC-SCPs had increased RAS activity at baseline relative to *NF1*$^{+/+}$ controls (**Supplemental Figure 2F**), the addition of Epidermal Growth Factor (EGF) further increased RAS-GFP levels in *NF1*$^{+/+}$ and *NF1*$^{+/-}$ hiPSC-SCPs, but not in *NF1*$^{-/-}$ hiPSC-SCPs (**Supplemental Figure 2F**)**.** This result demonstrates that *NF1* loss in SCPs results in maximal RAS activation. As a result, cell proliferation was maximally increased in *NF1*$^{-/-}$ hiPSC-SCPs (**Supplemental Figure 2G**). Western immunoblotting revealed increased expression of GAP43 **(Figure 2H and Supplemental Table 1)**, an essential marker for the cells of origin for neurofibroma, and slightly decreased expression of p53 **(Figure 2H and Supplemental Table 1)** important for regulating epithelial-mesenchymal transition (EMT) and stemness (27). Interestingly, we consistently observed increased expression of total ERK in *NF1*$^{-/-}$ hiPSC-SCPs **(Figure 2H)**. This increase in newly synthesized ERK might additionally influence tumor formation by elevating the pool of activatable ERK (28). Collectively,

these observations establish that *NF1* loss delays SLC differentiation, with *NF1*$^{+/-}$ and *NF1*$^{-/-}$ cells maintaining a more stem cell-like state, thus expanding the population of cells with the capacity to serve as the cells of origin for neurofibroma (4).

Next, we examined the impact of *Nf1* inactivation on mouse embryonic DRG/nerve root Schwann cell precursors (DNSCs, which contain the cells of origin for plexiform neurofibroma) (4) **(Supplemental Figure 2H, 2I)**. Adeno-Cre virus-infected *Nf1*$^{fl/fl}$ DNSCs, in which *Nf1* loss was confirmed at the DNA **(Supplemental Figure 2J)** and protein (**Figure 2I**) levels, had higher protein expression of the adult neural stem cell marker, nestin (**Figure 2I**) and higher mRNA levels of other stem cell markers (*Ednrb*, *Lgr5*, *Sox2*, *Ccnd2*, *Cd133*, *Igf2bp2*, *Lif*, *Olfm4*, and *Hopx*; **Figure 2J**), while concomitantly expressing lower mRNA levels of Schwann cell markers (*MPZ*, *ErbB3*, *p75*, *Ngfr*, *Sox10*, *Dhh*, *S100β* and *Krox20*; **Figure 2J**). We also observed that adeno-Cre virus-infected *Nf1*$^{fl/fl}$ DNSCs formed neurospheres, while GFP virus-infected *Nf1*$^{fl/fl}$ DNSCs did not form neurospheres following adenovirus infection **(Supplemental Figure 2K).** Similarly, *Nf1* loss resulted in higher RAS activity (**Supplemental Figure 2L**) and cell proliferation (**Supplemental Figure 2M**) relative to adeno-GFP virus-infected *Nf1*$^{fl/fl}$ DNSC controls. Mirroring our findings in the human SCPs, the addition of EGF further increased RAS activity in *Nf1*$^{fl/fl}$-GFP, but not in *Nf1*$^{fl/fl}$ adeno-Cre virus-infected DNSCs (**Supplemental Figure 2L**). In some neural lineages, *NF1* loss increases PI3K signaling in addition to MAPK signaling (29). However, we did not observe elevated phospho-S6 kinase levels in *Nf1*$^{-/-}$ DNSCs (**Figure 2I**). The higher GAP43 protein **(Figure 2I)** and mRNA **(Supplemental Figure 2N)** (~15 fold change) levels in Cre virus-infected *Nf1*$^{fl/fl}$ DNSCs were consistent with that observed in human *NF1*$^{-/-}$ iPSCs-SCPs **(Figure 2H)**. These results reveal precise coordination between proliferation and differentiation in SLC cells relevant to neurofibroma development.

hiPSCs with Patient *NF1* Mutations Generate Humanized Neurofibromas in Mice

During differentiation of hiPSCs into migrating neural crest cells and SCPs, we discovered that the homeobox protein, HOXb7, co-localized with SOX10 expression (**Figure 1**). Since we have previously shown that HOXb7 serves as a marker to trace the cells of

origin for neurofibromas in mice (6), we hypothesized that these differentiated hiPSC-SCPs contain the tumor-initiating cells that potentially could give rise to neurofibromas within a permissive microenvironment. To test this hypothesis, we implanted SOX10/HOXb7-expressing *NF1*$^{-/-}$ hiPSC-SCPs into the sciatic nerves of immunodeficient athymic (*nu/nu*) mice. These engrafted *NF1*$^{-/-}$ hiPSC-SCPs survived, proliferated, and formed *bona fide* masses (plexiform neurofibromas) that completely recapitulated all the histological features of human plexiform neurofibromas, including hypercellularity, disorganization of the nerve tissue architecture, and Schwann cells with wavy nuclei (**Figure 3A and B**). The neoplastic cells in these neurofibromas were immunopositive for the human-specific Ku80 marker, and all tumors contained S100β^{+}, GAP43^{+}, SOX10^{+}, HOXb7^{+} and Iba1^{+} (macrophage marker) cells (**Figure 3A, right sciatic nerve**) with co-localization of Ku80 and GAP43, and had increased levels of phosphorylated ERK and s6 when compared to control (**Figure 3A, left sciatic nerve**). These observations suggest that the neoplastic cells originated from the implanted *NF1*$^{-/-}$ hiPSC-SCPs that differentiated into GAP43^{+} SLCs within a favorable nerve microenvironment. In contrast, when SOX10/HOXb7-expressing *NF1*$^{+/-}$ hiPSC-SCPs were implanted into the left sciatic nerve, the Ku80^{+} patient-derived cells survived and differentiated into SLCs, but did not generate neurofibromas (**Figure 3A**), confirming that *NF1* loss is a requisite step for neurofibroma development. Interestingly, expression of the adult neural stem cell marker, Nestin, in addition to HOXb7, was seen in these human pNF lesions (**Figure 3B**), which mirrors the expression of Nestin, HOXb7, and SOX10 in hiPSC-SCPs (**Figure 1**) and in E13.5 DNSCs (**Figure 2**).

The Nerve Microenvironment Promotes NCSC Differentiation into Schwannian Lineage Cells and the Formation of Neurofibromas

Previous studies have revealed that the local nerve microenvironment is important for neurofibroma formation (30). To examine this requirement, we differentiated hiPSCs into neural crest stem cells (NCSCs), a precursor stage of SLCs, as confirmed by decreased expression of the Oct3/4 pluripotency marker and increased expression of NCSCs markers, p75 and HNK1 (**Figure 4A-C**). Although activation of the bone morphogenetic pathway (BMP) suppressed the specification of NCSCs (31), adding LDN193189, a

potent BMP inhibitor, did not increase the expression of NCSC markers (*e.g*., p75), as previously reported in mice (32).These differences might reflect endogenous BMP expression in hiPSCs lines (33) or the need for BMP during a critical developmental window in mice (34).

Importantly, when *NF1*$^{-/-}$ hiPSC-derived NCSCs (hiPSC-NCSCs) were subcutaneously implanted in *nu/nu* mice, we only observed cartilage formation (**Figure 4D and Supplemental Figure 3A**), another neural crest cell-derived tissue. This cartilage was positive for phospho-ERK indicating activation of MEK signaling and *NF1* loss (**Supplemental Figure 3A**). In striking contrast, *NF1*$^{-/-}$ hiPSC-NCSCs implanted into the sciatic nerve generated both cartilage and cNFs **(Figure 4E and Supplemental Figure 3**). However, *NF1*$^{+/+}$ hiPSC-NCSCs subcutaneously implanted or injected into left sciatic nerve of the same mice did not generate neurofibromas **(Figure 4E**). To determine whether there might be other cells present in the microenvironment that provided critical support for cNF development, we immunostained for fibroblast, endothelial cell, macrophage, and mast cell markers, but observed no obvious differences between subcutaneously and sciatic nerve-implanted hiPSC-NSCSs (**Supplemental Figure 3B**). These findings establish that while hiPSC-NCSCs can give rise to different neural crest derivatives, including chondrocytes and SLCs *in vivo*, consistent with previous work (35), the local nerve microenvironment is essential for the differentiation of *NF1*$^{-/-}$ NCSCs into SLCs and the formation of neurofibromas.

Benign Human-Derived Neurofibroma Transformation into MPNSTs

Neurofibroma progression to MPNST in NF1 patients occurs with a frequency of 8-15%, and is associated with additional genetic changes, including amplification/over-expression of oncogenic receptor tyrosine kinases (*EGFR*, *PDGFR, MET*) or growth factors (neuregulin-1, hepatocyte growth factor) coupled with the loss of tumor suppressor genes [*CDKN2A, PTEN, TP53,* or *components of the Polycomb Repressive Complex 2* (PRC2)] (36-47). To model genetic cooperativity between *NF1* loss and one of the other molecular events reported in human MPNSTs, we used CRISPR/Cas9 to mutate *TP53* in *NF1*$^{-/-}$ hiPSCs. Loss of NF1 and P53 expression in *NF1*$^{-/-}$ hiPSCs was confirmed by

western blot (**Figure 5A-B, Supplemental Figure 4A-B**) and qPCR (**Figure 5C and Supplemental Figure 4C**). As predicted, mRNA expression of the *TP53* target gene, *p21*, was likewise decreased (**Figure 5C and Supplemental Figure 4D**).

The pluripotency of *NF1*$^{-/-}$sg*TP53* hiPSCs was established by positive staining for NANOG, SOX2, and Oct3/4 (**Figure 5D**) and their ability to form teratomas (**Supplemental Figure 4E**). *NF1*$^{-/-}$sg*TP53* hiPSCs were differentiated to SCPs, confirmed by expression of AP2a, p75, GAP43, SOX10, and nestin proteins (**Figure 5D**), and increased mRNA levels of *HOXb7*, *SOX10*, *MPZ*, *CDH19*, *ITGA4*, *ErbB3, p75* and *GAP43* (**Figure 5E**). Although *NF1*$^{-/-}$sg*TP53* hiPSC-SCP proliferation was higher than observed in *NF1*$^{-/-}$*sgScr* hiPSC-SCPs (**Figure 5F**), the expression of SCP markers (*SOX10*, *MPZ*, *CDH19*, *p75*, *ITGA4*, and *ERBB3*) was lower **(Figure 5G**). In contrast, the expression of stem markers (*SOX2*, *SLUG*, *SNAIL*, and *TWIST*) was higher in *NF1*$^{-/-}$sg*TP53* hiPSC-SCPs relative to *NF1*$^{-/-}$*sgScr* hiPSC-SCPs **(Figure 5H).** Consistent with prior mouse modeling experiments, implantation of SOX10^{+} *NF1*$^{-/-}$sg*TP53* hiPSC-SCPs generated human MPNSTs similar to their human counterparts (Ku80^{+}, S100β^{+}, GAP43^{+}, SOX10^{+}, Ki67^{+} and mitotic marker phosphorylated Histone-3^{+} cells) (**Figure 6**). These findings suggest that maintenance of a stem cell or earlier Schwann cell lineage stage likely contributes to malignant transformation (48).

SOX10-Expressing Cells Contain Neurofibroma-Initiating Cells

Because SOX10 is highly expressed in both neurofibromas and MPNSTs **(Figures 3 and 6**), we hypothesized that SOX10-expressing cells contain the tumor-initiating cells that give rise to neurofibromas. This hypothesis is supported by the co-localization of SOX10 and HOXb7 in hiPSC-SCPs (**Figure 1**) and the observation that HOXb7 serves as a marker to trace the cells of origin for neurofibroma (6). To test this hypothesis, we depleted *Nf1* expression in SOX10 lineage–derived cells in mice by conditional transgenesis. Since *Nf1* inactivation in non-inducible (constitutive) *Sox10-Cre* mice results in neonatal lethality, we crossed tamoxifen-inducible *Sox10-CreERT2* mice with *Nf1*$^{fl/fl}$ mice to generate *Sox10-CreERT2; Nf1*$^{fl/fl}$ mice. Following tamoxifen treatment, LacZ was expressed in the spinal cord (**Supplemental Figure 5A**) and sciatic nerve

(**Supplemental Figure 5B**). We also confirmed tamoxifen-induced *Nf1* recombination (49) (**Supplemental Figure 5C**). By 6 months after tamoxifen exposure (9, 50), these mice began to show clinical signs characteristic of pNF development (scruffy fur, hunched back, limping, limb paralysis) (**Supplemental Figure 5D-E**), and had lower average body weights and worse survival compared to control mice **(Supplemental Figure 5F-G)**. We also consistently observed that mice in the $Nf1^{fl/-}$ group died from tumor development much faster than those in the $Nf1^{fl/fl}$ group (**Supplemental Figure 5G**). Spinal cord dissection revealed enlarged DRGs at the cervical, thoracic, and lumbar levels (**Figure 7A**). We also observed classic giant diffuse plexiform neurofibromas within the left hind limb, causing left leg gigantism in some *Sox10-CreERT2;* $Nf1^{fl/fl}$ mice **(Figure 7B)**. Histological and molecular analysis of these enlarged DRGs and legs demonstrated tumors that were immunopositive for S100β, GAP43, and SOX10 expression, as well as mast cell infiltration (**Figure 7**), similar to human pNFs (**Figure 3B**). *Nf1* loss in these tumors was confirmed by genotyping and western blot (**Supplemental Figure 5H-5I**).

Next, we examined the role of NF1 in Schwann cell differentiation *in vivo*. In contrast to control mice, tamoxifen-treated *Sox10-CreERT2; Nf1*-mutant ($Nf1^{fl/fl}$ or $Nf1^{fl/-}$) mice had more compact nerve bundles with fascicular tissue architecture **(Supplemental Figure 6A)**. Longitudinal sections of the sciatic nerves showed hypercellular, but well-organized, tissue architecture in *Nf1*-mutant mice **(Supplemental Figure 6A)**. The sciatic nerves of *Nf1*-mutant mice had multiple axons (TUBB3 stains axons) without myelin (MPZ stains myelin) **(Supplemental Figure 6B IV-IX)**, representing an undifferentiated stage. Transmission electron microscope (TEM) analysis further revealed that the sciatic nerves of normal mice had predominantly myelinated axons with one surrounding Schwann cell. However, the sciatic nerves of *Nf1*-mutant mice contain many unmyelinated/immature axons **(Supplemental Figure 6C III)**. Additionally, there were increased numbers of cells between myelinated axons in the *Nf1*-mutant nerves relative to controls **(Supplemental Figure 6C IV)**. These *in vivo* observations in *Nf1*-mutant mice are consistent with our *in vitro* observations (**Figure 2 and Supplemental Figure 2**) that *Nf1* loss impairs Schwann cell differentiation during development.

Temporal *Nf1* Deletion in SOX10$^+$ Cells Generates Nodular/Discrete Cutaneous Neurofibromas

In addition to developing plexiform neurofibroma, *Sox10-CreERT2; Nf1$^{fl/fl}$* mice also developed multiple discrete skin papules on their backs and necks (**Figure 8A and Supplemental Figure 7**). To determine whether these lesions were restricted to the dermis, we carefully dissected the skin to demonstrate that all tumors were exclusively confined to the dermis, as seen in human cNFs (**Supplemental Figure 7B**). In this respect, *Sox10-CreERT2; Nf1$^{fl/fl}$* mice recapitulated the characteristic body location, skin thickness, and cutaneous restriction of their human counterparts. Importantly, when *Sox10-CreERT2* expression was induced with tamoxifen in adult *Sox10-CreERT2; Nf1$^{fl/fl}$; R26-LacZ* mice older than 1 month of age, multiple nodules formed, which protruded from inside the skin (**Supplemental Figure 7B**), typical of human sessile cNFs (51). These tumors were more hypercellular relative to the adjacent "normal" skin (**Figure 8A - B**). The massive infiltration of LacZ$^+$ cells (**Figure 8A**) expressing SOX10 (**Figure 8A**) established that these neoplastic cells were of SOX10 lineage. The tumor area was also immunopositive for SLC markers (S100β, GAP43, SOX10), and contained Iba1$^+$ macrophages and numerous mast cells (**Figure 8A**), which was distinct from the adjacent "normal" skin (**Figure 8B**), similar to their human counterparts (**Figure 8C**).

The MEK inhibitor, selumetinib, was recently approved by the FDA for treatment of pNFs. To provide proof-of-principle support for the use of this novel genetically engineered mouse cNF model for future preclinical drug testing, we topically treated cNFs developing in *Sox10-CreERT2; R26-tdTomato* mice with the MEK inhibitor PD0325901 (PD901). A small cohort of mice (n=3 per group) were treated thrice daily for one week, but then became weak and sick, requiring euthanasia. Analysis of the tumors before and after treatment with PD901 demonstrated that MEK inhibition decreased ERK activity within the cNF (**Figure 8D-E**). Since these mice also harbor the R26-tdTomato Red reporter, we monitored the response of Sox10-Cre-positive cells to MEK inhibitor treatment using tdTomato Red signal. Consistent with reduced phospho-ERK immunostaining, there were reduced SOX10-positive (**Figure 8F**) and tdTomato Red-positive (**Figure 8G**) cells in the treated group compared to the before treatment or vehicle treatment groups. This proof-

of-principle experiment suggests that this murine cNF model may serve as a tractable platform for future preclinical drug studies.

Discussion

Cutaneous neurofibromas develop in nearly all individuals with NF1, can be disfiguring, and greatly affect quality of life. However, little is known about the mechanisms mediating their initiation and progression, and there are no effective medical treatments available. One of the barriers to the identification of promising therapies for cNFs has been the lack of suitable preclinical platforms. The studies presented here address this pressing need by generating robust hiPSC-derived neurofibroma and novel cNF mouse models. Using these systems, we discovered that *NF1* loss impairs Schwann cell lineage differentiation by maintaining a more stem-like state, which likely facilitates tumorigenesis. Moreover, deployment of a humanized model further underscored the critical importance of a permissive nerve microenvironment to human neurofibroma development. Taken together, the generation and authentication of these neurofibroma models establishes tractable platforms for future preclinical therapeutic discovery and testing.

SOX10^{+} stem cells contain the cells of origin for cutaneous and plexiform neurofibromas

Prior studies have established the importance of stem cells in the initiation and maintenance of a diverse number of blood and solid cancers (52, 53). Although stem cells constitute a small population, the acquisition of cancer-causing mutations favors a proliferative stage that facilitates tumor formation. Using patient-derived hiPSC-differentiated SCPs and mouse E13.5 DNCSs (containing neurofibroma cells of origin), we discovered that *NF1* loss impaired Schwann cell lineage differentiation by arresting cells in a more stem-like state, thus expanding the population of potential cells of origin for neurofibroma.

Using lineage tracing, we found that SOX10 was highly expressed in the dorsal root ganglion and sciatic nerve **(Supplemental Figure 5A and 5B)**, where the incidence of pNFs is highest. Consistent with this finding, neurofibroma-generating *NF1$^{-/-}$* hiPSC-SCPs **(Figure 1)** and humanized neurofibroma tissue **(Figure 3A)** highly express SOX10 (54).

Since we have previously shown that HOXb7 label the cells of origin for neurofibromas in mice (6) and HOXb7 co-localizes with SOX10 expression, we hypothesized that SOX10-expressing cells contain the tumor-initiating cells that give rise to neurofibromas. SOX10 is a transcription factor first expressed at E9.5 (55) and maintained throughout Schwann cell lineage differentiation (56), where it regulates the expression of Schwann cell lineage genes, including *Oct6* (57), *Krox20* (58), and *ErbB3* (59). Although SOX10 is not required for initial neural crest specification (59, 60), apoptosis of undifferentiated NCSCs and the failure of glial cell generation in the peripheral nerves of *SOX10*-mutant mice suggest a critical role for SOX10 in the maintenance of NCSC survival and in glial fate determination (61, 62). The high percentage of cNF and pNF co-occurrence in *SOX10-CreERT2; Nf1*$^{fl/fl}$ mice further underscores the importance of spatiotemporal *Nf1* loss in SOX10-expressing Schwann cell lineages for the formation of both cNF and pNF tumors. Importantly, we did not observe optic glioma (or other brain tumor) development in these mice **(Supplemental Figure 8)**, as seen in 15-20% of children with NF1 (63), since the cells of origin of these tumors are not SOX10^{+} cells (64).

Humanized NF Neurofibroma Models for Personalized Medicine

Histologically, human neurofibromas harbor both neoplastic S100β^{+} Schwann cells (*NF1*$^{-/-}$) and non-neoplastic elements (*NF1*$^{+/-}$ cells) in the tumor microenvironment (CD34^{+} fibroblasts, mast cells, and macrophages, nerve fibers) (22). These neuropathological features were faithfully recapitulated in the humanized neurofibroma model system and in the new murine cNF strain presented herein. Another notable feature of human neurofibromas is the formation of Meissner-like corpuscles (65), which was observed in the humanized patient-derived hiPSC pNF model (**Figure 3A**), which has not been previously observed in prior genetically engineered mouse models.

Relevant to human clinical trials targeting the neurofibroma tumor microenvironment (*e.g.*, Imatinib) (12) or the neoplastic Schwann cells (*e.g.*, MEK inhibitors) (66), tumor responses can vary greatly between patients. These observations argue for the development of robust authenticated preclinical systems to discover and evaluate potential personalized therapies. Unfortunately, primary tumor cells isolated from NF1

patient neurofibromas have limited proliferative capacity and do not form tumors when explanted in mice. Leveraging our prior experience in defining the cells of origin for cutaneous (6) and plexiform (4, 9, 50) neurofibromas in mice, we successfully employed hiPSCs to generate humanized models of NF1-associated neurofibromas. The availability of this humanized platform now permits an examination of potential factors that influence neurofibroma formation. One of these potential risk factors is the germline *NF1* gene mutation. In this regard, patients with specific germline NF1 gene mutations (Arg1809 missense mutations, c.2970_2972 deletion) fail to develop cutaneous or dermal neurofibromas (67, 68). Future studies using these patient-specific hiPSC lines will permit mechanistic studies aimed at defining how *NF1* gene mutations differentially promote tumor formation (20).

Taken together, we used converging human and mouse modeling methods to identify the common cells of origin for different types of neurofibroma and developed complementary models representing the full range of benign and malignant peripheral nerve sheath tumors. The use of these models as platforms to understand the molecular and cellular evolution of neurofibroma development, as well as for testing potential promising therapeutic compounds, will be of utmost importance in reducing the morbidity and mortality associated with these tumors in patients with NF1.

METHODS

Mice

Athymic nude mice were purchased from Charles River (Stock No: 490). The *Nf1*$^{fl/fl}$ mice have been previously described (1). For inducible conditional *Nf1* ablation, we used a tamoxifen-inducible Cre line, the *Sox10-CreERT2* transgenic mice from Jackson Laboratories (Stock No: 027651). For non-inducible conditional *Nf1* ablation, we used *Sox10-Cre* transgenic mice from Jackson Laboratories (Stock No: 025807). ROSA26-LacZ reporter mice were obtained from Jackson Laboratories.

Isogenic hiPSC Cell Generation and Culture

Commercially available BJFF.6 healthy human fibroblasts were reprogrammed into iPSCs (*NF1*$^{+/+}$) and were subsequently CRISPR/Cas9 engineered by the Washington University Genome Engineering and iPSC Core (GEiC) to harbor a heterozygous (*NF1*$^{+/-}$) or homozygous (*NF1*$^{-/-}$) *NF1* mutation found in NF1 patients: 6619C>T; c.6513T>A or c.2041C>T (20). hiPSCs were maintained in feeder-free, Matrigel-coated plates in mTeSR Plus medium (STEMCELL Technologies).

SCP Induction

SCP induction was performed using previously described protocols (69) with modifications. Briefly, hiPSCs were dissociated by Accutase (STEMCELL Technologies) and plated on Matrigel-coated plates at a density of 25,000 cells/cm^2 in mTeSR plus medium (STEMCELL Technologies) containing 10 μM ROCK inhibitor (STEMCELL Technologies). Differentiation was initiated by switching to SCPs differentiation medium (SCPs-DM) when the confluence was ~70%-80%. The SCPs-DM contained DMEM/F12 (Gibco), Basal Neural medium (Gibco), N2 (Gibco), B27 (Gibco), Glutamax (Corning), Non-essential amino acids (Corning), 2β-ME (Invitrogen), 50 ng/ml of neuregulin β-1 (Peprotech), 3 μM CHIR99021 (STEMCELL Technologies), and 10 μM SB431542 (EMD Millipore). The medium was changed every other day. The detailed information for each product is listed in **Supplemental Table 2.**

Neurosphere Assessment

Neurosphere assessments were performed using previously published protocols (19). The hiPSC-SCPs were dissociated by Accutase (STEMCELL Technologies) into single cell and suspended in SCPs-DM. The cells were plated into ultra-low 6-well plates (Corning) with 5X10^4 - 1X10^5 in 3 ml and allowed 6-14 days for neurosphere formation. The images of each neurosphere were captured by camera, and diameter of each neurosphere was measured in Photoshop. The average diameter of neurospheres from isogenic hiPSC-SCPs was calculated in Excel. The frequency of isogenic hiPSC-SCPs was assessed as the percentage of cells that could undergo self-renewal and form

multipotent neurospheres. Neurospheres and medium were transferred into 15 ml conical tubes and collected by centrifugation at 100Xg for 10 mins. After removing the supernatant and washing the cells with DPBS without Ca^{2+}/Mg^{2+}, the neurospheres were digested with 0.25%Trypsin/EDTA (Sigma) for 5 mins in a 37°C incubator. The neurospheres were gently triturated to create single cell suspensions. The number of cells needed to form neurospheres was counted using a hemocytometer (Fisher Scientific).

NCSC Induction

The NCSC induction protocol was optimized from previous publications (70). Briefly, hiPSCs were dissociated by Accutase (STEMCELL Technologies) and plated on Matrigel-coated plates at a density of 25,000 cells/cm^2 in mTeSR plus medium (STEMCELL Technologies) containing 10 μM ROCK inhibitor (STEMCELL Technologies). When cells reached 70% confluence, differentiation was initiated by switching to NCSC differentiation medium (NCSCs-DM) composed of DMEM/F12, 2% BSA (w/v), Glutamax, Non-essential amino acids, Trace A (Corning), Trace B (Corning), Trace C (Corning), 2β-ME (Invitrogen), 10 μg/ml Bovine transferrin (Invitrogen), 50 μg/ml (+)-sodium l-ascorbate (Sigma), 200 ng/ml LONGR3 IGF-I (Sigma), 10 ng/ml human recombinant FGF2 (Thermo Fisher), 8 ng/ml of neuregulin β-1 (Peprotech), 3 μM CHIR99021 (STEMCELL Technologies) and 10 μM SB431542 (EMD Millipore). The medium was changed every other day. Detailed information for each product is listed in **Supplemental Table 2.**

Implantation of Cells into the Sciatic Nerves of Immunocompromised Mice

Implantation of cells into the sciatic nerve was performed as previously described (4). Briefly, nude mice (*Foxn1*-mutant mice) were anesthetized (4 ul/g, body weight) using a mixture of ketamine (10 mg/ml) and xylazine (1 mg/ml) solution (provided by UT Southwestern ARC) by intraperitoneal injection. Using iris scissors, a skin incision was made above the femur. A pocket was formed, and the sciatic nerve was exposed by displacing the quadriceps muscle. 50 μl of L-15 medium containing 1×10^6 viable hiPSC-differentiated SCPs was then deposited into the pocket so that cells were in contact with the injured sciatic nerve. The quadriceps muscles was then closed with 4-0 Vicryl sutures

(Ethicon), and the skin was closed with staples. Mice were placed into warm cages to recover from anesthesia.

MEK Inhibitor Treatment

The MEK inhibitor PD0325901 (PD901) (Selleckchem) was dissolved in 100% DMSO (Sigma). Immediately before topical application, this solution was diluted 1:1 with water. 1 mg total of PD901 was applied to the backs of *Sox10-CreERT2; Nf1$^{fl/fl}$; R26-tdTomato* mice skin bearing cNFs thrice daily with inhibitor solution (3 mg total) or 50% DMSO (control). White petrolatum was used to occlude the inhibitor. Tumors were harvested for analysis after one week of treatment, when mice began to become weak and sick. Quantification of the *tdTomato Red*-positive cells was performed using ImageJ.

Fluorescence-Activated Cell Sorting (FACS)

NF1$^{+/+}$, *NF1*$^{+/-}$ and *NF1*$^{-/-}$ hiPSC-SCPs were dissociated using Accutase (STEMCELL technology) and resuspended in FACS buffer (DPBS without Ca^{2+}/Mg^{2+} containing 0.5 μM EDTA and 1% BSA) to a final concentration of 5X10^6 cells/ml. Non-specific staining of cells was blocked with human Fc block (BD Pharmingen) for 30 mins on ice. 200 μl of each sample was added to duplicate Falcon tubes for staining with APC-conjugated isotype control or APC-conjugated p75 antibodies for 1 hr on ice. Each sample was washed with FACS buffer twice and resuspended in 500 ul FACS buffer. After propidium iodide (PI) was added, the cell suspension was transferred to appropriate tubes for FACS. PI^-APC^+ cell population was analyzed by FlowJo.

Histology and Immunostaining

For hematoxylin and eosin (H&E) analysis, tissue specimens were harvested and fixed with 10% formalin in PBS for 1 day and subsequently embedded in paraffin. Sections (5 μm thick) were stained with H&E per manufacturer's protocol (StatLab). The antibodies used for immunohistochemistry and immunofluorescence studies are listed in **Supplemental Table 3**.

qPCR and Analysis

Total RNA was extracted using TRIzol Reagent (Life Tech), and 1 μg of RNA was reverse transcribed with an iScript™ Select cDNA Synthesis Kit (BIO-RAD). Primer sequences are listed in **Supplemental Table 4**. qRT-PCR mixtures were prepared with iTaq™ Universal SYBR Green Supermix (BIO-RAD) and reactions were performed on a CFX connect Real-time System (BIO-RAD). C_T values were normalized to the housekeeping gene beta-actin.

Plasmid construction

To silence *TP53* expression in *NF1*$^{-/-}$ hiPSCs, annealed sgRNAs targeting *TP53* were ligated to a digested CRISPRv2 vector. After transformation of the ligation product to Stbl3 competent cells and screening single clones on Ampicillin agar plates, the resulting clone was expanded in LB broth, and plasmids extracted using NucleoBond Xtra Midi (Macherey-Nagel). The sgRNA primers used are listed in **Supplemental Table 5**.

Genomic PCR

Genomic PCR was performed to identify the clones containing CRISPRv2 plasmids with the sgRNA insertion using 2XTaq RED Master Mix (Apex) and the primer sequences listed in **Supplemental Table 5**.

Genotyping

To determine the genotypes of genetically modified mice, genomic DNA was extracted from tails (pups) using 1 M Tris-HCl (PH=6.8) incubation for 1 hr followed by 50 mM NaOH neutralization. The DNA sequences including the target site were amplified with 2XTaq RED Master Mix (Apex). Primer sequences are listed in **Supplemental Table 6**.

4-hydroxytamoxifen and tamoxifen treatment

4-hydroxytamoxifen (Sigma-Aldrich) was dissolved in 100% ETOH at 4 mg/ml. P0 pups were injected subcutaneously with 40 μg/μl 4-hydroxytamoxifen. For adult mice, tamoxifen (Sigma-Aldrich) was dissolved in a sunflower oil/ethanol mixture (9:1) at 10 mg/ml. The mice were gavaged with 2 mg/200 μl tamoxifen for 5 consecutive days. Mice

were genotyped before and after injection to confirm the deletion of genes flanked by LoxP sites using the *Nf1* primers listed in **Supplemental Table 6**.

Statistical Analysis

Values for each sample were from at least three biologically independent experiments with at least three technical replicates. Data are reported as means ± SEM. Comparisons among groups were performed either by one-way ANOVA, two-way ANOVA or by two-tailed Student's *t* test for pair-wise comparisons. P values $\leqslant 0.05$ were considered statistically significant. *P< 0.05; **P < 0.01; ***P < 0.001; ****P < 0.0001.

Supplemental Table 7 lists the different genotypes of mice and their phenotypes.

Study approval

Animal care and use in this study were approved by the Institutional Animal Care and Use Committee at University of Texas Southwestern Medical Center.

Acknowledgements

We thank the members of the Le and Gutmann laboratories for helpful discussion, Yong Wang for technical assistance, and Renee McKay for reviewing and editing the manuscript. JM is the recipient of the Early Investigator Research Award from the US Department of Defense (W81XWH1910687), CA is funded by an NCI Research Specialist Award (R50CA233164). LQL holds the Thomas L. Shields, M.D. Professorship in Dermatology and is supported by the NF1 Research Consortium Fund and the Neurofibromatosis Therapeutic Acceleration Program. DHG holds the Donald O. Schnuck Family Professorship in Neurology. This work was supported by funding from the Giorgio Foundation (to LQL and DHG), the National Cancer Institute (R01 CA166593 to LQL), and the National Institutes of Health (R35 NS07211-01 to DHG).

Author Contributions:

Conception and design: LQL, JM, DHG

Development of methodology: LQL, JM, ZC

Acquisition of data (provided animals, generated cells and reagents, acquired data, provided facilities, etc.): LQL, JM, ZC, CA, TS, JP

Analysis and interpretation of data (e.g., statistical analysis, biostatistics, computational analysis): LQL, JM

Writing, review, and/or revision of the manuscript: LQL, JM, CA, DHG

Administrative, technical, or material support (i.e., reporting or organizing data, constructing databases): LQL, JM

Study supervision: LQL

References

1. Zhu Y, Ghosh P, Charnay P, Burns DK, and Parada LF. Neurofibromas in NF1: Schwann cell origin and role of tumor environment. *Science.* 2002;296(5569):920-2.

2. Zheng H, Chang L, Patel N, Yang J, Lowe L, Burns DK, et al. Induction of abnormal proliferation by nonmyelinating schwann cells triggers neurofibroma formation. *Cancer Cell.* 2008;13(2):117-28.

3. Wu J, Williams JP, Rizvi TA, Kordich JJ, Witte D, Meijer D, et al. Plexiform and dermal neurofibromas and pigmentation are caused by Nf1 loss in desert hedgehog-expressing cells. *Cancer Cell.* 2008;13(2):105-16.

4. Chen Z, Liu C, Patel AJ, Liao CP, Wang Y, and Le LQ. Cells of origin in the embryonic nerve roots for NF1-associated plexiform neurofibroma. *Cancer Cell.* 2014;26(5):695-706.

5. Mayes DA, Rizvi TA, Cancelas JA, Kolasinski NT, Ciraolo GM, Stemmer-Rachamimov AO, et al. Perinatal or adult Nf1 inactivation using tamoxifen-inducible PlpCre each cause neurofibroma formation. *Cancer Res.* 2011;71(13):4675-85.

6. Chen Z, Mo J, Brosseau JP, Shipman T, Wang Y, Liao CP, et al. Spatiotemporal Loss of NF1 in Schwann Cell Lineage Leads to Different Types of Cutaneous Neurofibroma Susceptible to Modification by the Hippo Pathway. *Cancer Discov.* 2019;9(1):114-29.

7. Radomska KJ, Coulpier F, Gresset A, Schmitt A, Debbiche A, Lemoine S, et al. Cellular Origin, Tumor Progression, and Pathogenic Mechanisms of Cutaneous

Neurofibromas Revealed by Mice with Nf1 Knockout in Boundary Cap Cells. *Cancer discovery.* 2019;9(1):130-47.

8. Brosseau JP, Liao CP, Wang Y, Ramani V, Vandergriff T, Lee M, et al. NF1 heterozygosity fosters de novo tumorigenesis but impairs malignant transformation. *Nat Commun.* 2018;9(1):5014.

9. Liao CP, Booker RC, Brosseau JP, Chen Z, Mo J, Tchegnon E, et al. Contributions of inflammation and tumor microenvironment to neurofibroma tumorigenesis. *J Clin Invest.* 2018;128(7):2848-61.

10. Yang FC, Ingram DA, Chen S, Zhu Y, Yuan J, Li X, et al. Nf1-dependent tumors require a microenvironment containing Nf1+/-- and c-kit-dependent bone marrow. *Cell.* 2008;135(3):437-48.

11. Hirbe AC, Dahiya S, Friedmann-Morvinski D, Verma IM, Clapp DW, and Gutmann DH. Spatially- and temporally-controlled postnatal p53 knockdown cooperates with embryonic Schwann cell precursor Nf1 gene loss to promote malignant peripheral nerve sheath tumor formation. *Oncotarget.* 2016;7(7):7403-14.

12. Robertson KA, Nalepa G, Yang FC, Bowers DC, Ho CY, Hutchins GD, et al. Imatinib mesylate for plexiform neurofibromas in patients with neurofibromatosis type 1: a phase 2 trial. *Lancet Oncol.* 2012;13(12):1218-24.

13. Ferguson MJ, Rhodes SD, Jiang L, Li X, Yuan J, Yang X, et al. Preclinical Evidence for the Use of Sunitinib Malate in the Treatment of Plexiform Neurofibromas. *Pediatr Blood Cancer.* 2016;63(2):206-13.

14. Gross AM, Wolters PL, Dombi E, Baldwin A, Whitcomb P, Fisher MJ, et al. Selumetinib in Children with Inoperable Plexiform Neurofibromas. *N Engl J Med.* 2020;382(15):1430-42.

15. Jessen KR, and Mirsky R. The origin and development of glial cells in peripheral nerves. *Nat Rev Neurosci.* 2005;6(9):671-82.

16. Riethmacher D, Sonnenberg-Riethmacher E, Brinkmann V, Yamaai T, Lewin GR, and Birchmeier C. Severe neuropathies in mice with targeted mutations in the ErbB3 receptor. *Nature.* 1997;389(6652):725-30.

17. Furlan A, Dyachuk V, Kastriti ME, Calvo-Enrique L, Abdo H, Hadjab S, et al. Multipotent peripheral glial cells generate neuroendocrine cells of the adrenal medulla. *Science.* 2017;357(6346).

18. Joseph NM, Mukouyama YS, Mosher JT, Jaegle M, Crone SA, Dormand EL, et al. Neural crest stem cells undergo multilineage differentiation in developing

peripheral nerves to generate endoneurial fibroblasts in addition to Schwann cells. *Development.* 2004;131(22):5599-612.

19. Joseph NM, Mosher JT, Buchstaller J, Snider P, McKeever PE, Lim M, et al. The loss of Nf1 transiently promotes self-renewal but not tumorigenesis by neural crest stem cells. *Cancer Cell.* 2008;13(2):129-40.

20. Anastasaki C, Wegscheid ML, Hartigan K, Papke JB, Kopp ND, Chen J, et al. Human iPSC-Derived Neurons and Cerebral Organoids Establish Differential Effects of Germline NF1 Gene Mutations. *Stem Cell Reports.* 2020.

21. Schmid RS, McGrath B, Berechid BE, Boyles B, Marchionni M, Sestan N, et al. Neuregulin 1-erbB2 signaling is required for the establishment of radial glia and their transformation into astrocytes in cerebral cortex. *Proc Natl Acad Sci U S A.* 2003;100(7):4251-6.

22. Le LQ, Shipman T, Burns DK, and Parada LF. Cell of origin and microenvironment contribution for NF1-associated dermal neurofibromas. *Cell Stem Cell.* 2009;4(5):453-63.

23. Bollag G, Clapp DW, Shih S, Adler F, Zhang YY, Thompson P, et al. Loss of NF1 results in activation of the Ras signaling pathway and leads to aberrant growth in haematopoietic cells. *Nat Genet.* 1996;12(2):144-8.

24. Chen YH, Gianino SM, and Gutmann DH. Neurofibromatosis-1 regulation of neural stem cell proliferation and multilineage differentiation operates through distinct RAS effector pathways. *Genes Dev.* 2015;29(16):1677-82.

25. Hegedus B, Dasgupta B, Shin JE, Emnett RJ, Hart-Mahon EK, Elghazi L, et al. Neurofibromatosis-1 regulates neuronal and glial cell differentiation from neuroglial progenitors in vivo by both cAMP- and Ras-dependent mechanisms. *Cell Stem Cell.* 2007;1(4):443-57.

26. Iwashita T, Kruger GM, Pardal R, Kiel MJ, and Morrison SJ. Hirschsprung disease is linked to defects in neural crest stem cell function. *Science.* 2003;301(5635):972-6.

27. Schubert J, and Brabletz T. p53 Spreads out further: suppression of EMT and stemness by activating miR-200c expression. *Cell Res.* 2011;21(5):705-7.

28. Xue JY, Zhao Y, Aronowitz J, Mai TT, Vides A, Qeriqi B, et al. Rapid non-uniform adaptation to conformation-specific KRAS(G12C) inhibition. *Nature.* 2020;577(7790):421-5.

29. Johannessen CM, Reczek EE, James MF, Brems H, Legius E, and Cichowski K. The NF1 tumor suppressor critically regulates TSC2 and mTOR. *Proc Natl Acad Sci U S A.* 2005;102(24):8573-8.

30. Liao CP, Pradhan S, Chen Z, Patel AJ, Booker RC, and Le LQ. The role of nerve microenvironment for neurofibroma development. *Oncotarget.* 2016;7(38):61500-8.

31. Menendez L, Yatskievych TA, Antin PB, and Dalton S. Wnt signaling and a Smad pathway blockade direct the differentiation of human pluripotent stem cells to multipotent neural crest cells. *Proc Natl Acad Sci U S A.* 2011;108(48):19240-5.

32. McMahon JA, Takada S, Zimmerman LB, Fan CM, Harland RM, and McMahon AP. Noggin-mediated antagonism of BMP signaling is required for growth and patterning of the neural tube and somite. *Genes Dev.* 1998;12(10):1438-52.

33. Hackland JOS, Frith TJR, Thompson O, Navarro AM, Garcia-Castro MI, Unger C, et al. Top-Down Inhibition of BMP Signaling Enables Robust Induction of hPSCs Into Neural Crest in Fully Defined, Xeno-free Conditions. *Stem Cell Reports.* 2017;9(4):1043-52.

34. Mica Y, Lee G, Chambers SM, Tomishima MJ, and Studer L. Modeling Neural Crest Induction, Melanocyte Specification, and Disease-Related Pigmentation Defects in hESCs and Patient-Specific iPSCs. *Cell Reports.* 2013;3(4):1140-52.

35. Carrio M, Mazuelas H, Richaud-Patin Y, Gel B, Terribas E, Rosas I, et al. Reprogramming Captures the Genetic and Tumorigenic Properties of Neurofibromatosis Type 1 Plexiform Neurofibromas. *Stem Cell Reports.* 2019;12(2):411-26.

36. Cichowski K, Shih TS, Schmitt E, Santiago S, Reilly K, McLaughlin ME, et al. Mouse Models of Tumor Development in Neurofibromatosis Type 1. *Science.* 1999;286(5447):2172-6.

37. Endo M, Kobayashi C, Setsu N, Takahashi Y, Kohashi K, Yamamoto H, et al. Prognostic Significance of p14ARF, p15INK4b, and p16INK4a Inactivation in Malignant Peripheral Nerve Sheath Tumors. *Clinical Cancer Research.* 2011;17(11):3771-82.

38. Gregorian C, Nakashima J, Dry SM, Nghiemphu PL, Smith KB, Ao Y, et al. PTEN dosage is essential for neurofibroma development and malignant transformation. *Proceedings of the National Academy of Sciences.* 2009;106(46):19479-84.

39. Huijbregts RPH, Roth KA, Schmidt RE, and Carroll SL. Hypertrophic Neuropathies and Malignant Peripheral Nerve Sheath Tumors in Transgenic Mice

Overexpressing Glial Growth Factor β3 in Myelinating Schwann Cells. *The Journal of Neuroscience.* 2003;23(19):7269-80.

40. Joseph NM, Mosher JT, Buchstaller J, Snider P, McKeever PE, Lim M, et al. The Loss of Nf1 Transiently Promotes Self-Renewal but Not Tumorigenesis by Neural Crest Stem Cells. *Cancer Cell.* 2008;13(2):129-40.

41. Keng VW, Rahrmann EP, Watson AL, Tschida BR, Moertel CL, Jessen WJ, et al. PTEN and NF1 Inactivation in Schwann Cells Produces a Severe Phenotype in the Peripheral Nervous System That Promotes the Development and Malignant Progression of Peripheral Nerve Sheath Tumors. *Cancer Research.* 2012;72(13):3405-13.

42. Ling BC, Wu J, Miller SJ, Monk KR, Shamekh R, Rizvi TA, et al. Role for the epidermal growth factor receptor in neurofibromatosis-related peripheral nerve tumorigenesis. *Cancer Cell.* 2005;7(1):65-75.

43. Perrone F, Da Riva L, Orsenigo M, Losa M, Jocollè G, Millefanti C, et al. PDGFRA, PDGFRB, EGFR, and downstream signaling activation in malignant peripheral nerve sheath tumor. *Neuro-Oncology.* 2009;11(6):725-36.

44. PERRY A, KUNZ SN, FULLER CE, BANERJEE R, MARLEY EF, LIAPIS H, et al. Differential NF1, p16, and EGFR Patterns by Interphase Cytogenetics (FISH) in Malignant Peripheral Nerve Sheath Tumor (MPNST) and Morphologically Similar Spindle Cell Neoplasms. *Journal of Neuropathology & Experimental Neurology.* 2002;61(8):702-9.

45. Torres KE, Zhu Q-S, Bill K, Lopez G, Ghadimi MP, Xie X, et al. Activated MET Is a Molecular Prognosticator and Potential Therapeutic Target for Malignant Peripheral Nerve Sheath Tumors. *Clinical Cancer Research.* 2011;17(12):3943-55.

46. Vogel KS, Klesse LJ, Velasco-Miguel S, Meyers K, Rushing EJ, and Parada LF. Mouse Tumor Model for Neurofibromatosis Type 1. *Science.* 1999;286(5447):2176-9.

47. Lee W, Teckie S, Wiesner T, Ran L, Prieto Granada CN, Lin M, et al. PRC2 is recurrently inactivated through EED or SUZ12 loss in malignant peripheral nerve sheath tumors. *Nature genetics.* 2014;46(11):1227-32.

48. Miller SJ, Rangwala F, Williams J, Ackerman P, Kong S, Jegga AG, et al. Large-scale molecular comparison of human schwann cells to malignant peripheral nerve sheath tumor cell lines and tissues. *Cancer Res.* 2006;66(5):2584-91.

49. Zhu Y, Romero MI, Ghosh P, Ye Z, Charnay P, Rushing EJ, et al. Ablation of NF1 function in neurons induces abnormal development of cerebral cortex and reactive gliosis in the brain. *Genes Dev.* 2001;15(7):859-76.

50. Le LQ, Liu C, Shipman T, Chen Z, Suter U, and Parada LF. Susceptible stages in Schwann cells for NF1-associated plexiform neurofibroma development. *Cancer Res.* 2011;71(13):4686-95.

51. Chamseddin BH, Hernandez L, Solorzano D, Vega J, and Le LQ. Robust surgical approach for cutaneous neurofibroma in neurofibromatosis type 1. *JCI insight.* 2019;5.

52. Eppert K, Takenaka K, Lechman ER, Waldron L, Nilsson B, van Galen P, et al. Stem cell gene expression programs influence clinical outcome in human leukemia. *Nat Med.* 2011;17(9):1086-93.

53. Ricci-Vitiani L, Lombardi DG, Pilozzi E, Biffoni M, Todaro M, Peschle C, et al. Identification and expansion of human colon-cancer-initiating cells. *Nature.* 2007;445(7123):111-5.

54. Antonescu CR SB, Woodruff JM. *AFIP atlas of tumor pathology.* ARP Press; 2013.

55. Pusch C, Hustert E, Pfeifer D, Sudbeck P, Kist R, Roe B, et al. The SOX10/Sox10 gene from human and mouse: sequence, expression, and transactivation by the encoded HMG domain transcription factor. *Hum Genet.* 1998;103(2):115-23.

56. Jessen KR, and Mirsky R. Schwann Cell Precursors; Multipotent Glial Cells in Embryonic Nerves. *Front Mol Neurosci.* 2019;12:69.

57. Finzsch M, Schreiner S, Kichko T, Reeh P, Tamm ER, Bosl MR, et al. Sox10 is required for Schwann cell identity and progression beyond the immature Schwann cell stage. *J Cell Biol.* 2010;189(4):701-12.

58. Schreiner S, Cossais F, Fischer K, Scholz S, Bosl MR, Holtmann B, et al. Hypomorphic Sox10 alleles reveal novel protein functions and unravel developmental differences in glial lineages. *Development.* 2007;134(18):3271-81.

59. Britsch S, Goerich DE, Riethmacher D, Peirano RI, Rossner M, Nave KA, et al. The transcription factor Sox10 is a key regulator of peripheral glial development. *Genes Dev.* 2001;15(1):66-78.

60. Southard-Smith EM, Kos L, and Pavan WJ. Sox10 mutation disrupts neural crest development in Dom Hirschsprung mouse model. *Nat Genet.* 1998;18(1):60-4.

61. Paratore C, Goerich DE, Suter U, Wegner M, and Sommer L. Survival and glial fate acquisition of neural crest cells are regulated by an interplay between the

transcription factor Sox10 and extrinsic combinatorial signaling. *Development.* 2001;128(20):3949-61.

62. Sonnenberg-Riethmacher E, Miehe M, Stolt CC, Goerich DE, Wegner M, and Riethmacher D. Development and degeneration of dorsal root ganglia in the absence of the HMG-domain transcription factor Sox10. *Mech Dev.* 2001;109(2):253-65.

63. Campen CJ, and Gutmann DH. Optic Pathway Gliomas in Neurofibromatosis Type 1. *J Child Neurol.* 2018;33(1):73-81.

64. Lee DY, Gianino SM, and Gutmann DH. Innate neural stem cell heterogeneity determines the patterning of glioma formation in children. *Cancer Cell.* 2012;22(1):131-8.

65. Ortonne N, Wolkenstein P, Blakeley JO, Korf B, Plotkin SR, Riccardi VM, et al. Cutaneous neurofibromas: Current clinical and pathologic issues. *Neurology.* 2018;91(2 Suppl 1):S5-S13.

66. Dombi E, Baldwin A, Marcus LJ, Fisher MJ, Weiss B, Kim A, et al. Activity of Selumetinib in Neurofibromatosis Type 1-Related Plexiform Neurofibromas. *N Engl J Med.* 2016;375(26):2550-60.

67. Rojnueangnit K, Xie J, Gomes A, Sharp A, Callens T, Chen Y, et al. High Incidence of Noonan Syndrome Features Including Short Stature and Pulmonic Stenosis in Patients carrying NF1 Missense Mutations Affecting p.Arg1809: Genotype-Phenotype Correlation. *Human mutation.* 2015;36(11):1052-63.

68. Koczkowska M, Callens T, Gomes A, Sharp A, Chen Y, Hicks AD, et al. Expanding the clinical phenotype of individuals with a 3-bp in-frame deletion of the NF1 gene (c.2970_2972del): an update of genotype-phenotype correlation. *Genet Med.* 2019;21(4):867-76.

69. Kim HS, Lee J, Lee DY, Kim YD, Kim JY, Lim HJ, et al. Schwann Cell Precursors from Human Pluripotent Stem Cells as a Potential Therapeutic Target for Myelin Repair. *Stem cell reports.* 2017;8(6):1714-26.

70. Menendez L, Kulik MJ, Page AT, Park SS, Lauderdale JD, Cunningham ML, et al. Directed differentiation of human pluripotent cells to neural crest stem cells. *Nat Protoc.* 2013;8(1):203-12.

Figure 1

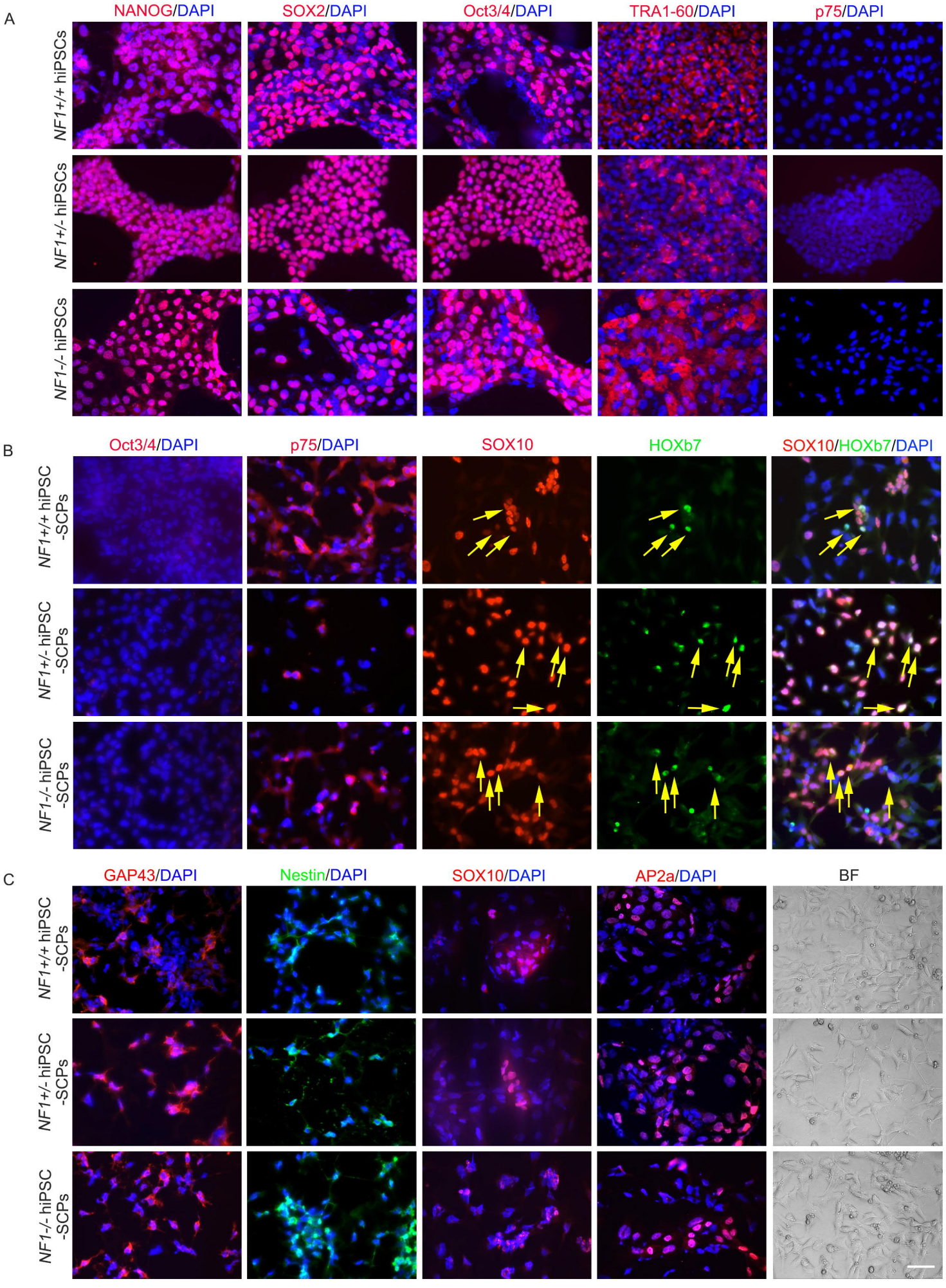
A
NANOG/DAPI
SOX2/DAPI
Oct3/4/DAPI
TRA1-60/DAPI
p75/DAPI
NF1+/+ hiPSCs
NF1+/- hiPSCs
NF1-/- hiPSCs
B
Oct3/4/DAPI
p75/DAPI
SOX10
HOXb7
SOX10/HOXb7/DAPI
NF1+/+ hiPSC -SCPs
NF1+/- hiPSC -SCPs
NF1-/- hiPSC -SCPs
C
GAP43/DAPI
Nestin/DAPI
SOX10/DAPI
AP2a/DAPI
BF
NF1+/+ hiPSC -SCPs
NF1+/- hiPSC -SCPs
NF1-/- hiPSC -SCPs

Figure 1. Differentiation of hiPSCs to SCPs. (A) Pluripotency of isogenic *NF1+/+*, *NF1+/-* and *NF1-/-* hiPSCs was confirmed by expression of NANOG, Oct3/4, SOX2, and TRA1-60. **(B)** Differentiation of isogenic hiPSCs to SCPs was confirmed by negative staining for Oct3/4 at day 6, and positive staining for p75, SOX10, and HOXb7 at day 10. **(C)** Differentiation of isogenic hiPSCs to SCPs was confirmed by positive staining for GAP43 and nestin at day 10, and for SOX10 and AP2a at day 20, respectively. The morphology was distinct from original hiPSCs 10 days after differentiation. Yellow arrows depict the co-localization of SOX10 and HOXb7 in hiPSC-SCPs (B). BF: Bright field. Scale bar, 50 μm.

Figure 2

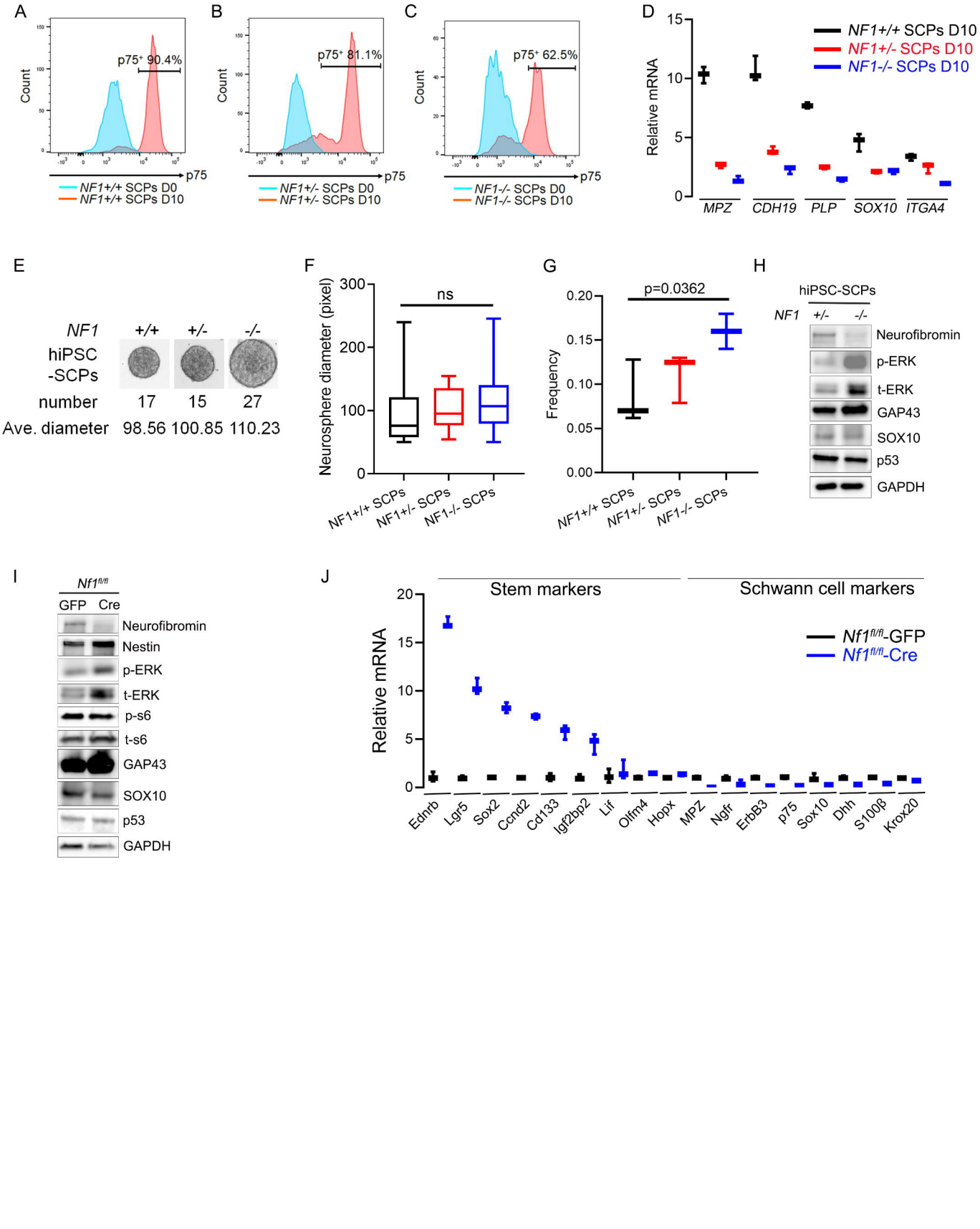
A
B
C
D
Count
p75⁺ 90.4%
p75⁺ 81.1%
p75⁺ 62.5%
p75
NF1+/+ SCPs D0
NF1+/+ SCPs D10
NF1+/- SCPs D0
NF1+/- SCPs D10
NF1-/- SCPs D0
NF1-/- SCPs D10
Relative mRNA
NF1+/+ SCPs D10
NF1+/- SCPs D10
NF1-/- SCPs D10
MPZ
CDH19
PLP
SOX10
ITGA4
E
NF1
+/+
+/-
-/-
hiPSC -SCPs
number 17 15 27
Ave. diameter 98.56 100.85 110.23
F
Neurosphere diameter (pixel)
ns
NF1+/+ SCPs
NF1+/- SCPs
NF1-/- SCPs
G
Frequency
p=0.0362
H
hiPSC-SCPs
NF1 +/- -/-
Neurofibromin
p-ERK
t-ERK
GAP43
SOX10
p53
GAPDH
I
Nf1fl/fl
GFP Cre
Neurofibromin
Nestin
p-ERK
t-ERK
p-s6
t-s6
GAP43
SOX10
p53
GAPDH
J
Stem markers
Schwann cell markers
Relative mRNA
Nf1fl/fl-GFP
Nf1fl/fl-Cre
Ednrb
Lgr5
Sox2
Ccnd2
Cd133
Igf2bp2
Lif
Olfm4
Hopx
MPZ
Ngfr
ErbB3
p75
Sox10
Dhh
S100β
Krox20

Figure 2. *NF1* loss impairs Schwann cell differentiation by maintaining stemness. **(A-C)** Flow cytometry was performed to measure the percentage of $p75^{+}$ cells after differentiation. **(D)** mRNA levels for SCP markers, including *MPZ*, *CDH19*, *PLP*, *SOX10*, and *ITGA4* were compared in *NF1+/+*, *NF1+/-* and *NF1-/-* hiPSC-SCPs. (**E-G)** hiPSCs were grown in SCP-DM for 4 days, followed by suspension culture for an extra 6-14 days. Neurosphere numbers **(E)** were counted and the average diameters (n = 15-27/group) **(F)** calculated. Comparisons among groups were performed by one-way ANOVA. **(G)** Frequencies of isogenic hiPSC-SCPs were assessed as the percentage of cells that formed neurospheres. Comparisons among groups were performed by one-way ANOVA. **(H)** Neurofibromin, phospho-$ERK^{Thr202/Thr204}$ (p-ERK), total-ERK (t-ERK), GAP43, SOX10, and p53 expression by Western blot in *NF1+/-* and *NF1-/-* hiPSC-SCPs, with GAPDH as an internal loading control. **(I)** Protein expression of neurofibromin, Nestin, p-ERK, t-ERK, phospho-$S6^{Ser240/244}$ (p-s6), total-S6 (t-s6), GAP43, SOX10, and p53 was measured by Western blot in adeno-GFP virus-infected and adeno-Cre virus-infected E13.5 $Nf1^{fl/fl}$ DNSCs. **(J)** The mRNA levels of stem markers (*Ednrb*, *Lgr5*, *Sox2*, *Ccnd2*, *Cd133*, *Igf2bp2*, *Lif*, *Olfm4*, and *Hopx)* and *Schwann cell* markers (*MPZ*, *Ngfr*, *ErbB3*, *p75*, *Sox10*, *Dhh*, *S100β* and *Krox20*) were compared between GFP adenovirus-infected and Cre adenovirus-infected E13.5 $Nf1^{f/f}$ DNSCs. Box and whisker plots were performed in **D**, **F**, **G** and **J**. Box plots show median (line), lower quartile and upper quartile (box). The end of the whiskers represents the lower and highest observation of all the data. Comparisons among groups were performed by one-way ANOVA. ns, not significant.

Figure 3

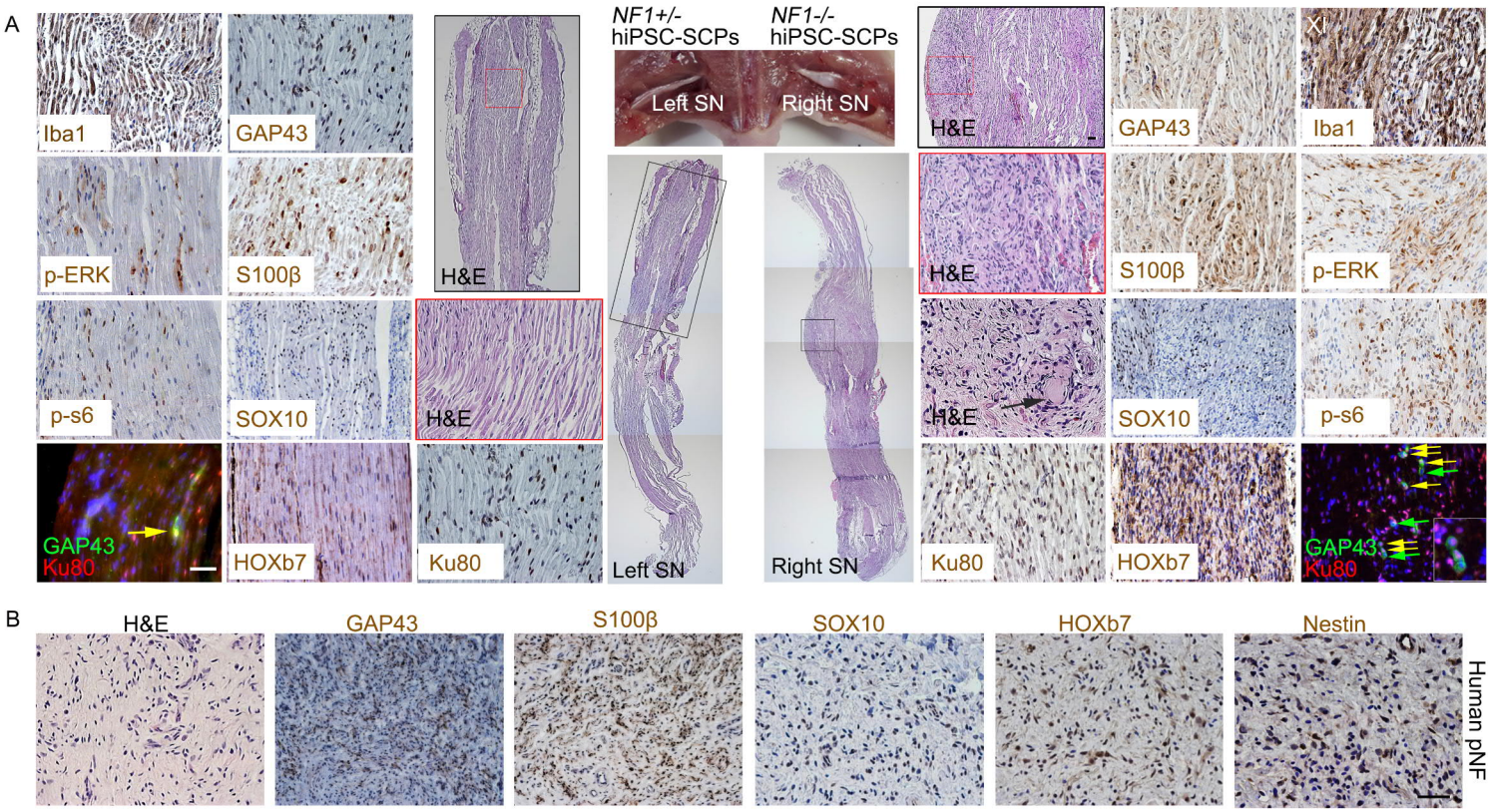
A
Iba1
GAP43
p-ERK
S100β
p-s6
SOX10
GAP43
Ku80
HOXb7
H&E
Ku80
H&E
NF1+/-
hiPSC-SCPs
NF1-/-
hiPSC-SCPs
Left SN
Right SN
Left SN
Right SN
H&E
H&E
H&E
Ku80
GAP43
S100β
SOX10
HOXb7
Iba1
p-ERK
p-s6
GAP43
Ku80
B
H&E
GAP43
S100β
SOX10
HOXb7
Nestin
Human pNF

Figure 3. *NF1-/-* hiPSC-SCPs give rise to pNFs. (A) The non-tumor-bearing left sciatic nerve injected with *NF1+/-* hiPSC-SCPs and the right neurofibroma-bearing sciatic nerve injected with *NF1-/-* hiPSC-SCPs were fully characterized by H&E, immunostaining with the human-specific Ku80, GAP43, S100β, SOX10, HOXb7, p-ERK, p-s6 and Iba1 antibodies. Yellow arrows show the co-localization of $GAP43^{+}$ and $Ku80^{+}$ cells. Green arrows show $GAP43^{+}Ku80^{-}$ cells. Black arrow shows the Meissner-like corpuscle in the neurofibroma. n = 5. **(B)** Characterization of human plexiform neurofibroma tissue by H&E, immunostaining for GAP43, S100β, SOX10, HOXb7, and Nestin. SN: Sciatic nerve. Scale bar, 50 μm.

Figure 4

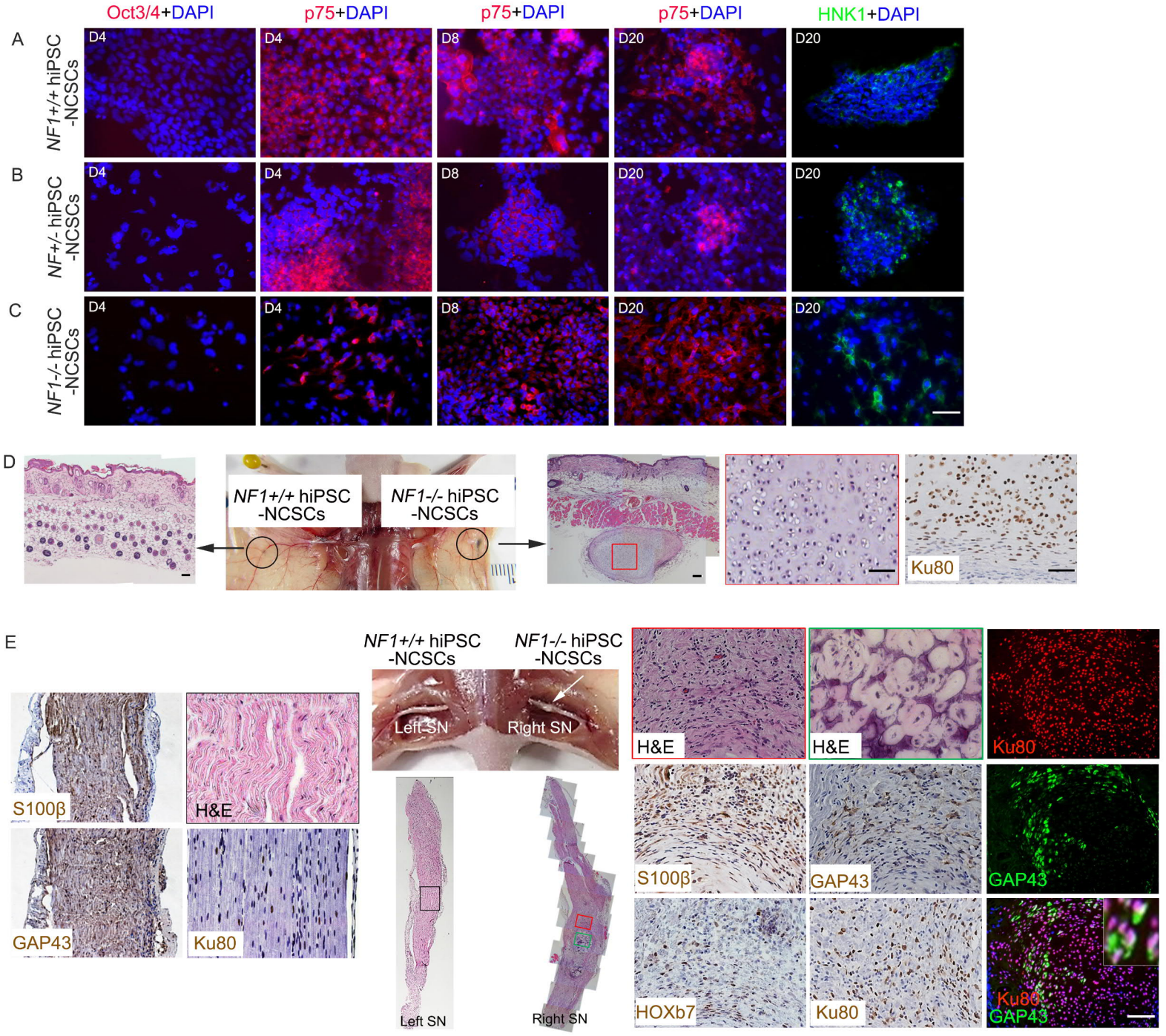
Oct3/4+DAPI
p75+DAPI
p75+DAPI
p75+DAPI
HNK1+DAPI
A
NF1+/+ hiPSC -NCSCs
B
NF+/- hiPSC -NCSCs
C
NF1-/- hiPSC -NCSCs
D4
D8
D20
D
NF1+/+ hiPSC -NCSCs
NF1-/- hiPSC -NCSCs
Ku80
E
S100β
H&E
GAP43
Ku80
Left SN
Right SN
HOXb7

Figure 4. The nerve microenvironment promotes NCSC differentiation into Schwann cell lineage cells and the formation of neurofibromas. (A-C) After differentiation, hiPSC-NCSCs were immunonegative for Oct3/4 at day 4, immunopositive for p75 at day 4, day 8 and day 20, and immunopositive for HNK1 at day 20. **(D)** Patient-derived hiPSC-NCSCs were subdermally injected into athymic mice. Formation of cartilage derived from injected $Ku80^{+}$ cells was observed under the skin following *NF1-/-* hiPSC-NCSC implantation, but not in the left side after *NF1+/+* hiPSC-NCSC implantation. n = 3. **(E)** Patient-derived hiPSC-NCSCs were injected into the sciatic nerves of athymic mice. Formation of cartilage and tumor with neurofibroma histological and molecular characteristics were observed in the right sciatic nerves following implantation of *NF1-/-* hiPSC-NCSCs . Co-localization of Ku80 and GAP43 was observed. The left sciatic nerve injected with *NF1+/+* hiPSC-NCSCs was immunopositive for Ku80, but still well-organized without histological features of neurofibroma. n = 3. White arrow points to tumor in right sciatic nerve. SN, Sciatic nerve. Scale bar, 50 μm.

Figure 5

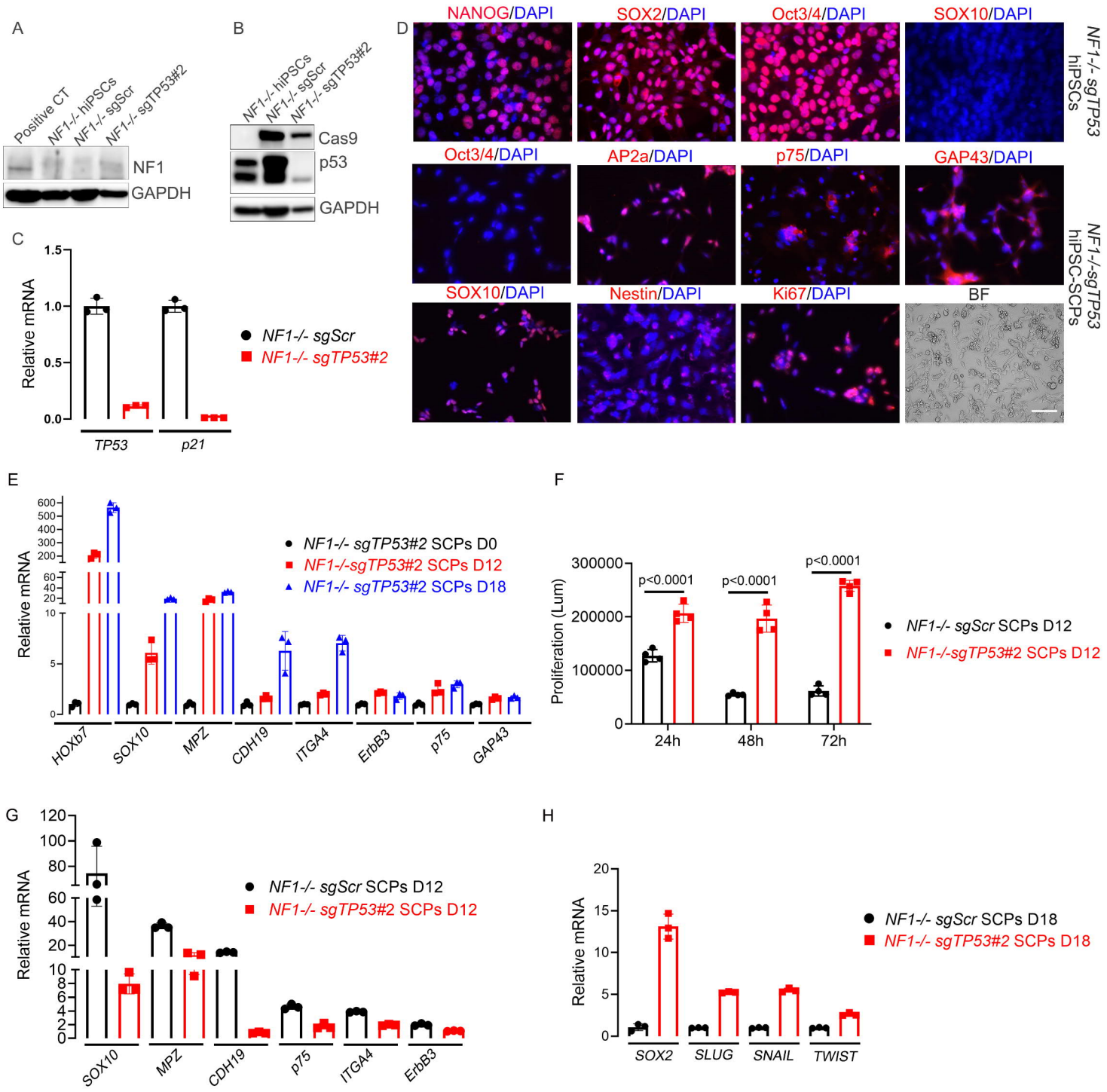
A
Positive CT
NF1-/- hiPSCs
NF1-/- sgScr
NF1-/- sgTP53#2
NF1
GAPDH
B
NF1-/- hiPSCs
NF1-/- sgScr
NF1-/- sgTP53#2
Cas9
p53
GAPDH
C
Relative mRNA
1.5
1.0
0.5
0.0
TP53
p21
NF1-/- sgScr
NF1-/- sgTP53#2
D
NANOG/DAPI
SOX2/DAPI
Oct3/4/DAPI
SOX10/DAPI
NF1-/- sgTP53 hiPSCs
Oct3/4/DAPI
AP2a/DAPI
p75/DAPI
GAP43/DAPI
SOX10/DAPI
Nestin/DAPI
Ki67/DAPI
BF
NF1-/-sgTP53 hiPSC-SCPs
E
Relative mRNA
600
500
400
300
200
60
40
20
10
5
0
NF1-/- sgTP53#2 SCPs D0
NF1-/-sgTP53#2 SCPs D12
NF1-/- sgTP53#2 SCPs D18
HOXb7
SOX10
MPZ
CDH19
ITGA4
ErbB3
p75
GAP43
F
Proliferation (Lum)
300000
200000
100000
0
p<0.0001
p<0.0001
p<0.0001
24h
48h
72h
NF1-/- sgScr SCPs D12
NF1-/-sgTP53#2 SCPs D12
G
Relative mRNA
120
100
80
60
40
20
10
8
6
4
2
0
NF1-/- sgScr SCPs D12
NF1-/- sgTP53#2 SCPs D12
SOX10
MPZ
CDH19
p75
ITGA4
ErbB3
H
Relative mRNA
20
15
10
5
0
SOX2
SLUG
SNAIL
TWIST
NF1-/- sgScr SCPs D18
NF1-/- sgTP53#2 SCPs D18

Figure 5. Differentiation of patient-derived hiPSC with loss of *NF1* and *TP53* to Schwann cell precursors. (A-B) *TP53* loss was genetically engineered using CRISPR/Cas9 in *NF1-/-* hiPSCs. Expression of neurofibromin, Cas9, and TP53 were measured by Western blot. GAPDH was used as an internal loading control. **(C)** qPCR was performed to measure mRNA levels of *TP53* and *p21* in *NF1-/- sgTP53* hiPSCs. **(D)** After editing and single cell clone selection, *NF1-/- sgTP53* hiPSCs retain pluripotency, as verified by expression of pluripotent markers (NANOG, SOX2, and Oct3/4). However, SCP marker SOX10 was negative. Differentiation of *NF1-/- sgTP53* hiPSCs into SCPs was confirmed by fluorescent staining using SCP markers (SOX10, AP2a, p75, GAP43 and nestin). **(E)** mRNA levels of indicated SCP markers were measured. **(F)** Cell proliferation was compared between *NF1-/- sgScr* hiPSC-SCPs and *NF1-/- sgTP53* hiPSC-SCPs using the cell titer glow assay. Comparisons between groups were performed by two-way ANOVA. **(G-H)** The mRNA levels of SCP markers and stem markers were compared between *NF1-/- sgScr* hiPSC-SCPs and *NF1-/- sgTP53* hiPSC-SCPs. BF: Bright field. Scale bar, 50 μm.

Figure 6

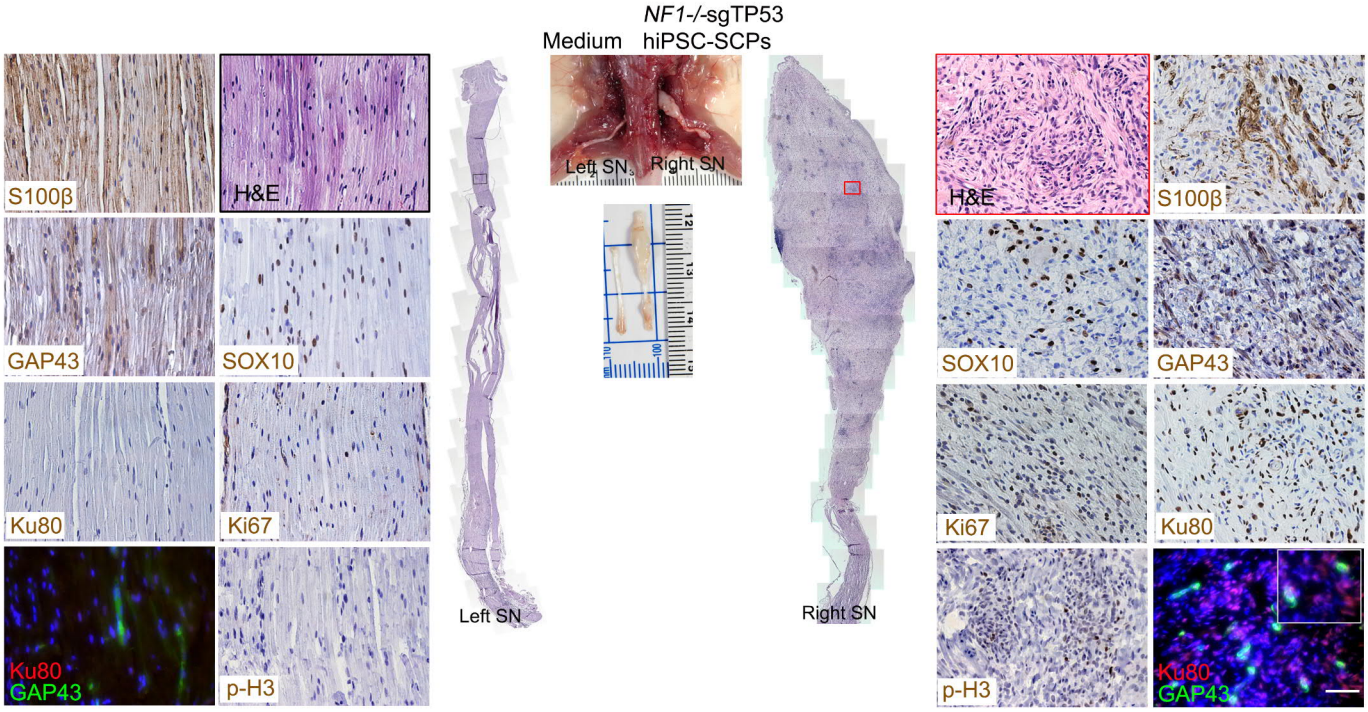
Medium
NF1-/-sgTP53 hiPSC-SCPs
Left SN
Right SN
S100β
H&E
GAP43
SOX10
Ku80
Ki67
Ku80 GAP43
p-H3
Left SN
Right SN
H&E
S100β
SOX10
GAP43
Ki67
Ku80
p-H3
Ku80 GAP43

Figure 6. Loss of *NF1* and *TP53* in patient-derived hiPSC-SCPs drives MPNST development. After implantation of *NF1-/- sgTP53* hiPSC-SCPs into the right sciatic nerve, MPNSTs were observed and characterized by H&E, S100β, SOX10, GAP43 , Ki67, Ku80 and phospho-H3 expression. Insert shows the co-localization of $GAP43^{+}$ and $Ku80^{+}$ cells. The left sciatic nerve injected with medium served as a control. n = 3.; SN: Sciatic nerve. Scale bar, 50 μm.

Figure 7

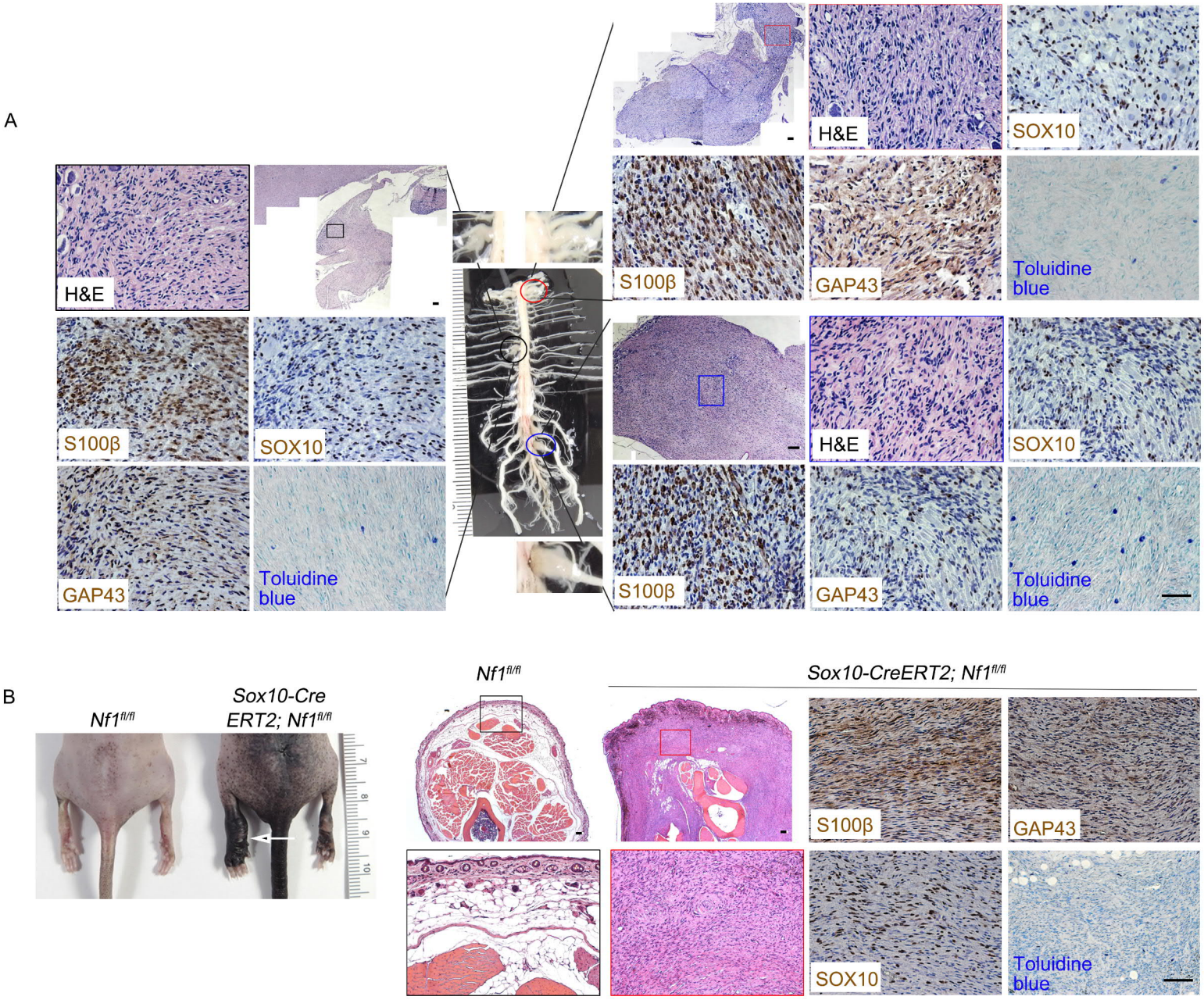
A
H&E
S100β
SOX10
GAP43
Toluidine blue
B
Nf1fl/fl
Sox10-Cre ERT2; Nf1fl/fl
Sox10-CreERT2; Nf1fl/fl

Figure 7. SOX10-expressing cells contain proliferating tumorigenic cells for pNF. **(A)** *Sox10-CreERT2; Nf1*$^{fl/fl}$ mice treated with tamoxifen demonstrated neurofibroma formation, characterized by abnormally enlarged DRGs, as well as hypercellular and disorganized DRGs. The pNF was positive for S100β, GAP43, and SOX10 expression, with infiltration of mast cells. **(B)** A representative *Sox10-CreERT2; Nf1*$^{fl/fl}$ mouse treated with tamoxifen developed classic giant diffuse plexiform neurofibromas (white arrow) with hyperpigmentation, thickening of the skin, which was positive for S100β, GAP43, and SOX10 expression with mast cell infiltration. n = 43. Scale bar, 50 μm.

Figure 8

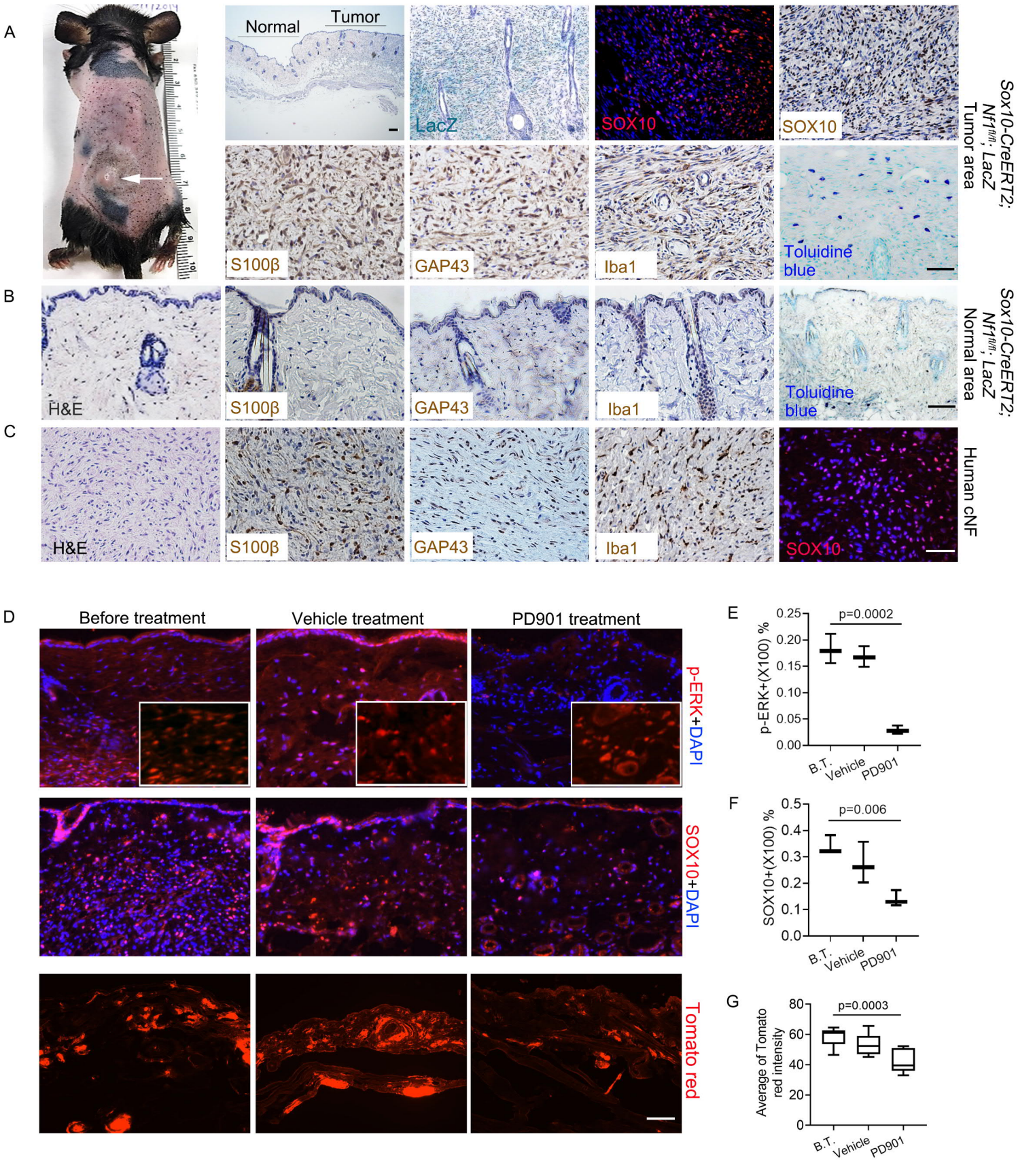
A
Normal
Tumor
LacZ
SOX10
SOX10
S100β
GAP43
Iba1
Toluidine blue
Sox10-CreERT2; Nf1fl/fl; LacZ Tumor area
B
H&E
S100β
GAP43
Iba1
Toluidine blue
Sox10-CreERT2; Nf1fl/fl; LacZ Normal area
C
H&E
S100β
GAP43
Iba1
SOX10
Human cNF
D
Before treatment
Vehicle treatment
PD901 treatment
p-ERK+DAPI
SOX10+DAPI
Tomato red
E
p=0.0002
p-ERK+(X100) %
0.25
0.20
0.15
0.10
0.05
0.00
B.T.
Vehicle
PD901
F
p=0.006
SOX10+(X100) %
0.5
0.4
0.3
0.2
0.1
0.0
B.T.
Vehicle
PD901
G
p=0.0003
Average of Tomato red intensity
80
60
40
20
0
B.T.
Vehicle
PD901

Figure 8. SOX10-expressing cells contain proliferating tumorigenic cells for cNF. **(A)** *Sox10-CreERT2; Nf1$^{fl/fl}$* mice gradually developed discrete cutaneous neurofibromas (white arrow), characterized by increased skin thickness, positive staining for SOX10, S100β, GAP43, and Iba1, with mast cell infiltration. **(B)** The area distant from the tumor sites of discrete cutaneous neurofibromas was characterized by S100β, GAP43, and Iba1 expression, and toluidine blue staining. **(C)** cNF patient tissue was positive for S100β, GAP43, Iba1, and SOX10. n = 38. Scale bar, 50 μm. **(D)** Cutaneous NF tumors from *Sox10-CreERT2; Nf1$^{fl/f}$; R26-tdTomato* mice before MEK inhibitor treatment, treated with vehicle, and treated with the MEK inhibitor PD0325901 (PD901) were harvested and stained for phospho-ERK (p-ERK); total-ERK (t-ERK, inserts) and SOX10. n = 3 per treatment group. **(E)** Quantification of p-ERK-positive cells. Comparisons among groups were performed by one-way ANOVA. **(F)** Quantification of SOX10-positive cells. Comparisons among groups were performed by one-way ANOVA. **(G)** Quantification of tdTomato Red intensity. n = 7-9/group. Comparisons among groups were performed by one-way ANOVA. Box and whisker plots were performed in **E**, **F**, and **G**. Box plots show median (line), lower quartile and upper quartile (box). The end of the whiskers represents the lower and highest observation of all the data.

Supplemental Figure 1

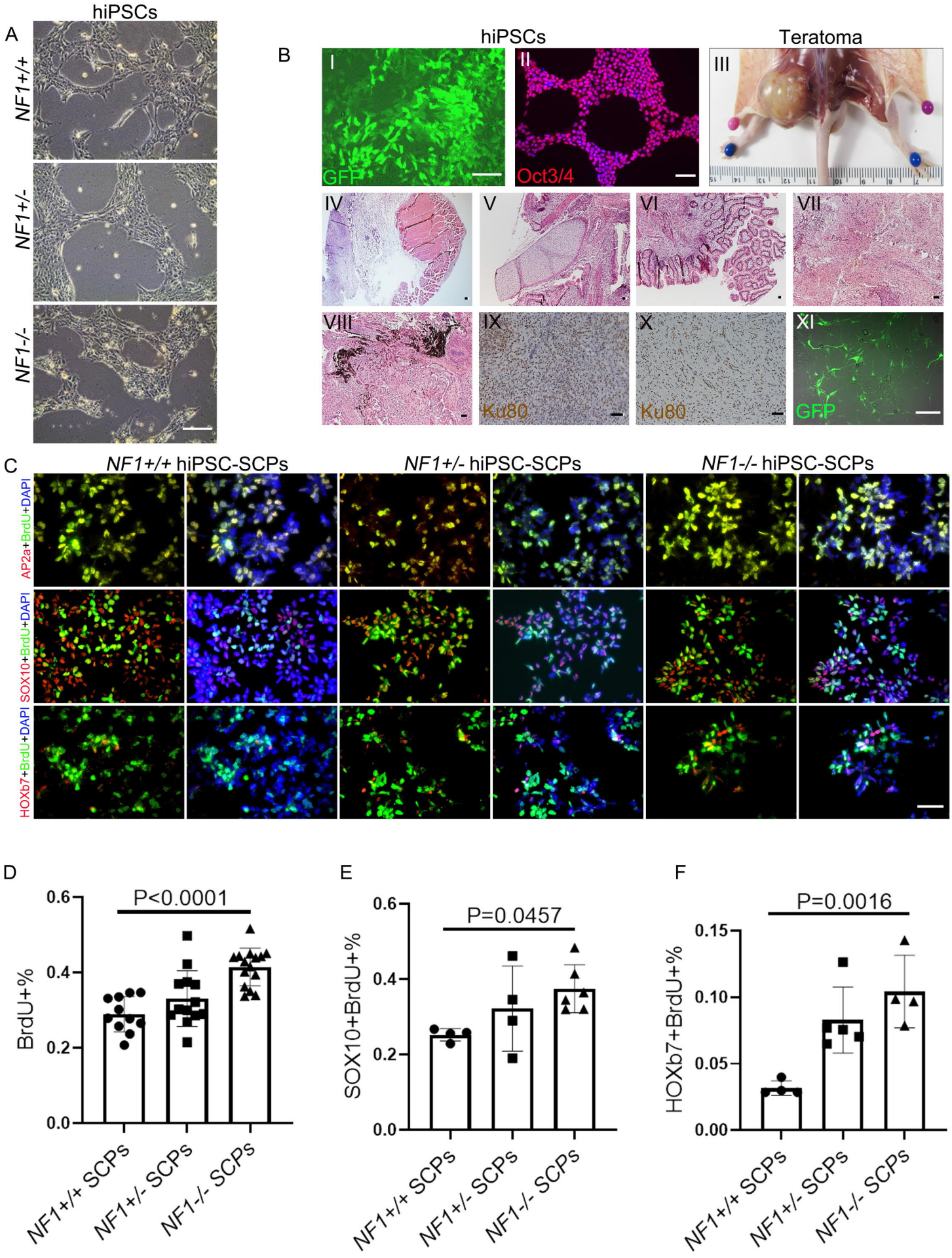

Supplemental Figure 1. Characterization of a series of isogenic hiPSCs and differentiated SCPs that harbor mutations observed in patients with NF1 (related to Figure 1). (A) Bright field images of *NF1+/+*, *NF1+/-*, and *NF1-/-* hiPSCs. **(B)** GFP-tagged hiPSCs (I and II) were injected into athymic mice. (II is a lower magnification image of the Oct3/4 image shown in the Fig. 1A *NF1+/-*hiPSCs Oct3/4 DAPI panel.) The representative teratoma (III) was characterized by H&E and the human specific antibody Ku80. The formation of fat tissue (IV), cartilage (V), luminal-like structures (VI), blood vessels (VII), pigmentation (VIII) and positive staining for Ku80 (IX was teratoma and X was human tissue as positive control) confirmed the pluripotency of hiPSCs. The cells isolated from teratoma (XI) were positive for GFP (XI). n = 3. Scale bar, 50 μm. **(C)** After incubation with BrdU, hiPSC-SCPs were double stained for BrdU and SCP markers including AP2α, SOX10, and HOXb7. Scale bar, 50 μm. **(D)** The percentage of BrdU, SOX10+BrdU+, and HOXb7+BrdU+ cells was calculated and compared between *NF1+/+*, *NF1+/-*, and *NF1-/-* hiPSC-SCPs. Comparisons among groups were performed by one-way ANOVA.

Supplemental Figure 2

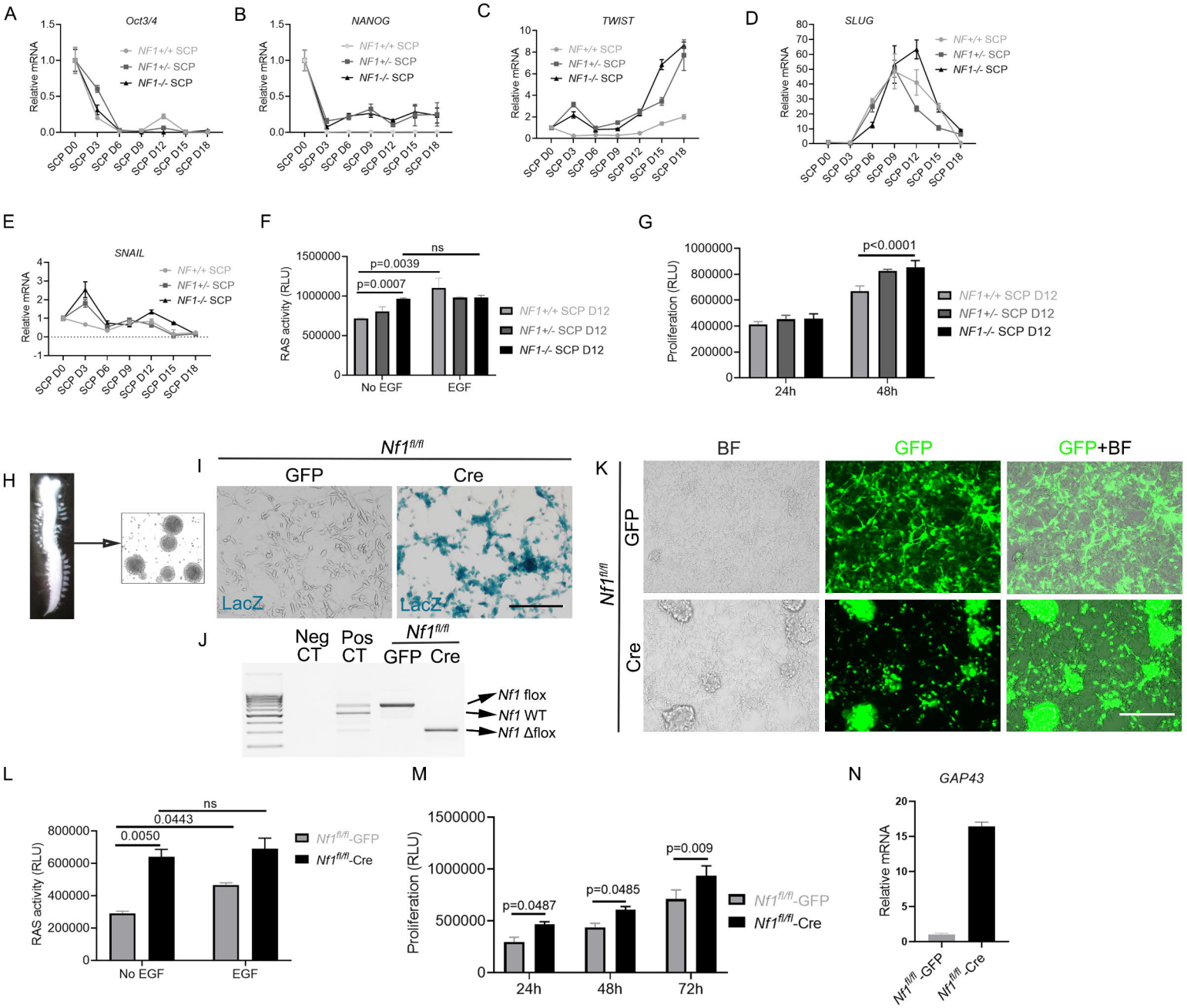

Supplemental Figure 2. *NF1* loss impairs Schwann cell differentiation by maintaining stemness (related to Figure 2). (A-B) mRNA levels of *Oct3/4* and *NANOG* in *NF1+/+*, *NF1+/-*, and *NF1-/-* hiPSC-SCPs were measured. **(C-E)** mRNA levels for migrating NCSCs (*TWIST*, *SLUG*, and *SNAIL*) in *NF1+/+*, *NF1+/-*, and *NF1-/-* hiPSC-SCPs were compared. **(F)** RAS activity was compared between isogenic hiPSC-SCPs with or without EGF. Comparisons between groups were performed by two-way ANOVA. **(G)** Cell proliferation was compared between isogenic hiPSC-SCPs using the cell titer glow assay. Comparisons among groups were performed by one-way ANOVA. **(H)** DNSCs were isolated from E13.5 embryos and formed neurospheres in suspension culture. **(I)** After adenovirus infection, cells were stained with X-gal. The $LacZ^{+}$ staining in adeno-Cre virus-infected E13.5 $Nf1^{fl/fl}$ DNSCs confirmed *Nf1* deletion. **(J)** *Nf1* deletion was demonstrated by PCR. **(K)** GFP expression was compared between GFP and Cre adenovirus-infected E13.5 $Nf1^{fl/fl}$ DNSCs. **(L)** RAS activity was compared between GFP and Cre adenovirus-infected E13.5 $Nf1^{f/f}$ DNSCs with or without EGF. **(M)** Cell proliferation was compared between GFP and Cre adenovirus-infected E13.5 $NF1^{fl/fl}$ DNSCs using the cell titer glow assay. Comparisons between groups were performed by two-way ANOVA. **(N)** mRNA levels of *GAP43* were compared between GFP and Cre adenovirus-infected E13.5 $Nf1^{f/f}$ DNSCs. Comparisons among groups were performed by one-way ANOVA. Scale bar, 50 μm.

Supplemental Figure 3

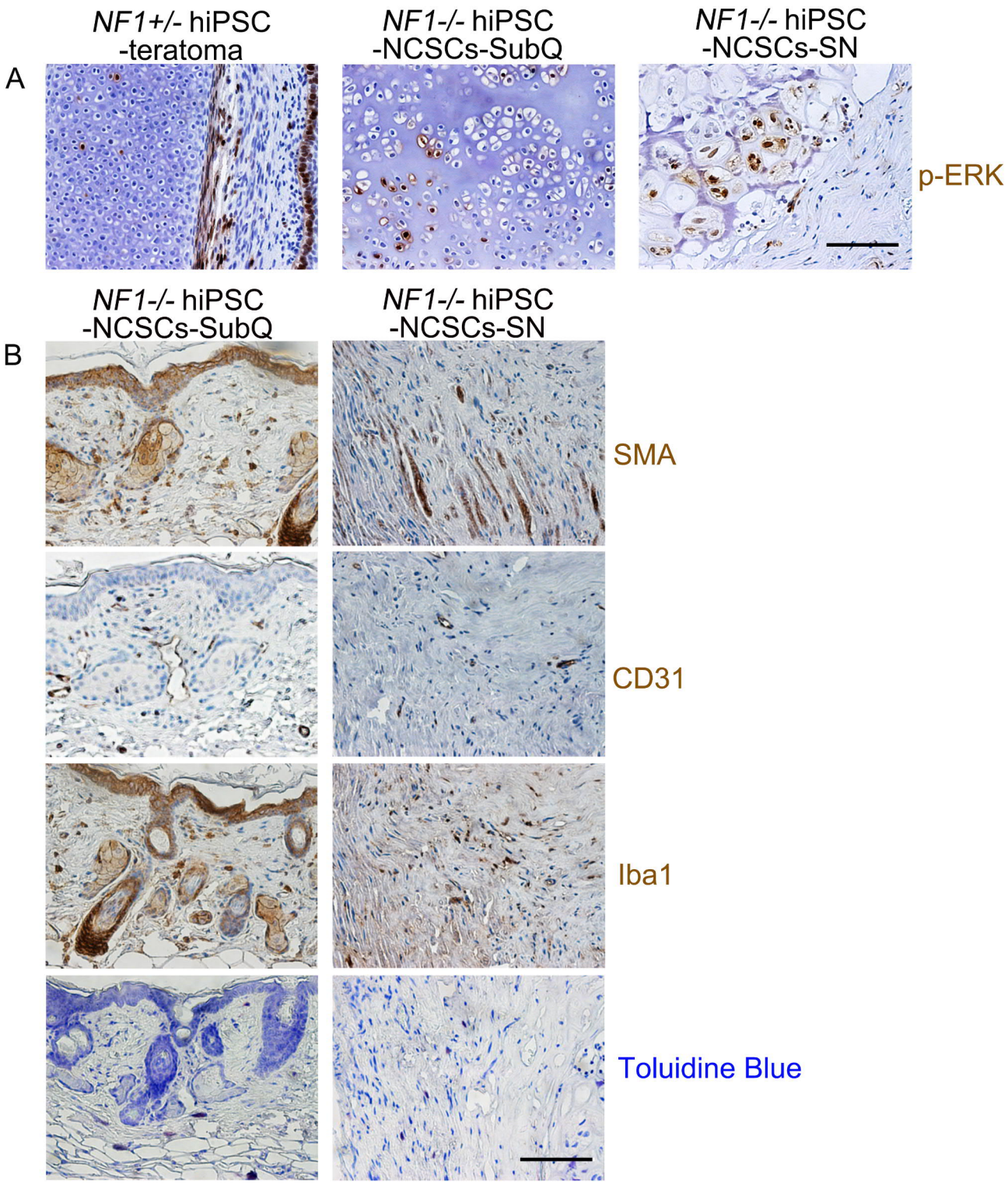

Supplemental Figure 3. Characterization of neurofibroma and cartilage formation (related to Figure 4). (A) Immunostaining of the indicated tissue injected with hiPSCs or hiPSC-NCSCs for expression of phospho-ERK (p-ERK). SubQ = subcutaneous; SN = sciatic nerve. **(B)** Immunostaining of the indicated tissue injected with *NF1-/-* hiPSC-NCSCs for expression of SMA (fibroblasts), CD31 (endothelial cells), Iba1 (macrophages), and Toluidine Blue (mast cells). n = 3. Scale bar, 50 μm.

Supplemental Figure 4

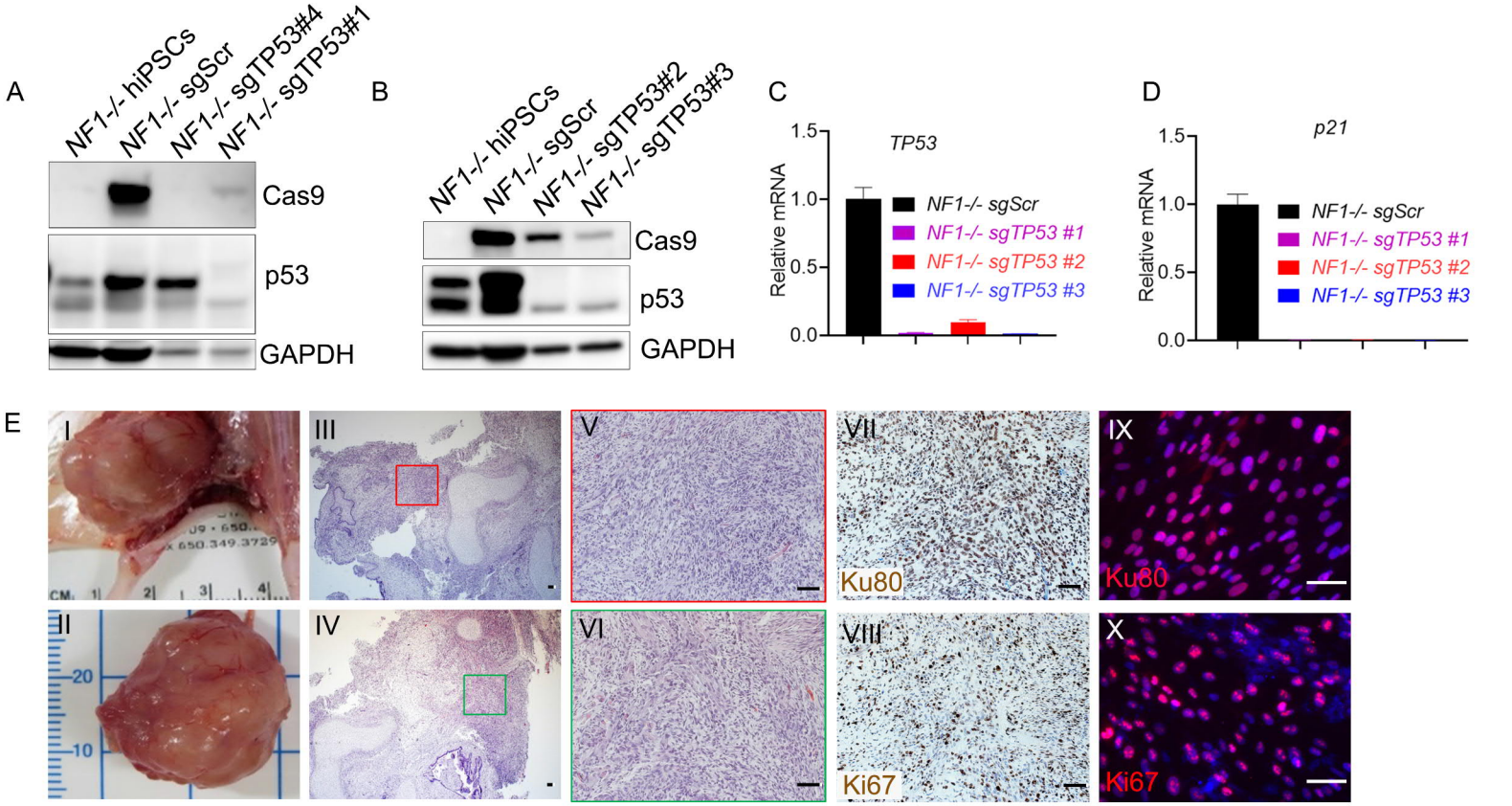

Supplemental Figure 4. Generation and characterization of *NF1-/- sgTP53* hiPSCs (related to Figure 5). (A) Expression of Cas9 and p53 were measured by Western blot. GAPDH was used as a loading control. *NF1-/-* sgTP53#4 failed because Cas9 was not successfully transfected. *TP53* deletion in *NF1-/-* sgTP53#1 was confirmed. **(B)** Expression of Cas9 and p53 were measured by Western blot. GAPDH was used as an internal loading control. *TP53* deletion in *NF1-/-* sgTP53#2 and #3 was confirmed. (Same blot as shown in Fig. 5B, but also showing the additional lane with *NF1-/-* sgTP53#3.) **(C-D)** mRNA levels of *TP53* and *p21* were measured before and after CRISPR/Cas9 engineered *TP53* deletion. **(E)** CRISPR/Cas9 engineered *NF1-/- sgTP53* hiPSCs were injected into athymic mice. Cartilage (III and IV), luminal-like structures (III and IV) and hypercellularity (V and VI) were observed in representative teratomas (I and II), which were positive for Ku80 (VII and IX) and Ki67 (VIII and X). n = 3. Scale bar, 50 μm.

Supplemental Figure 5

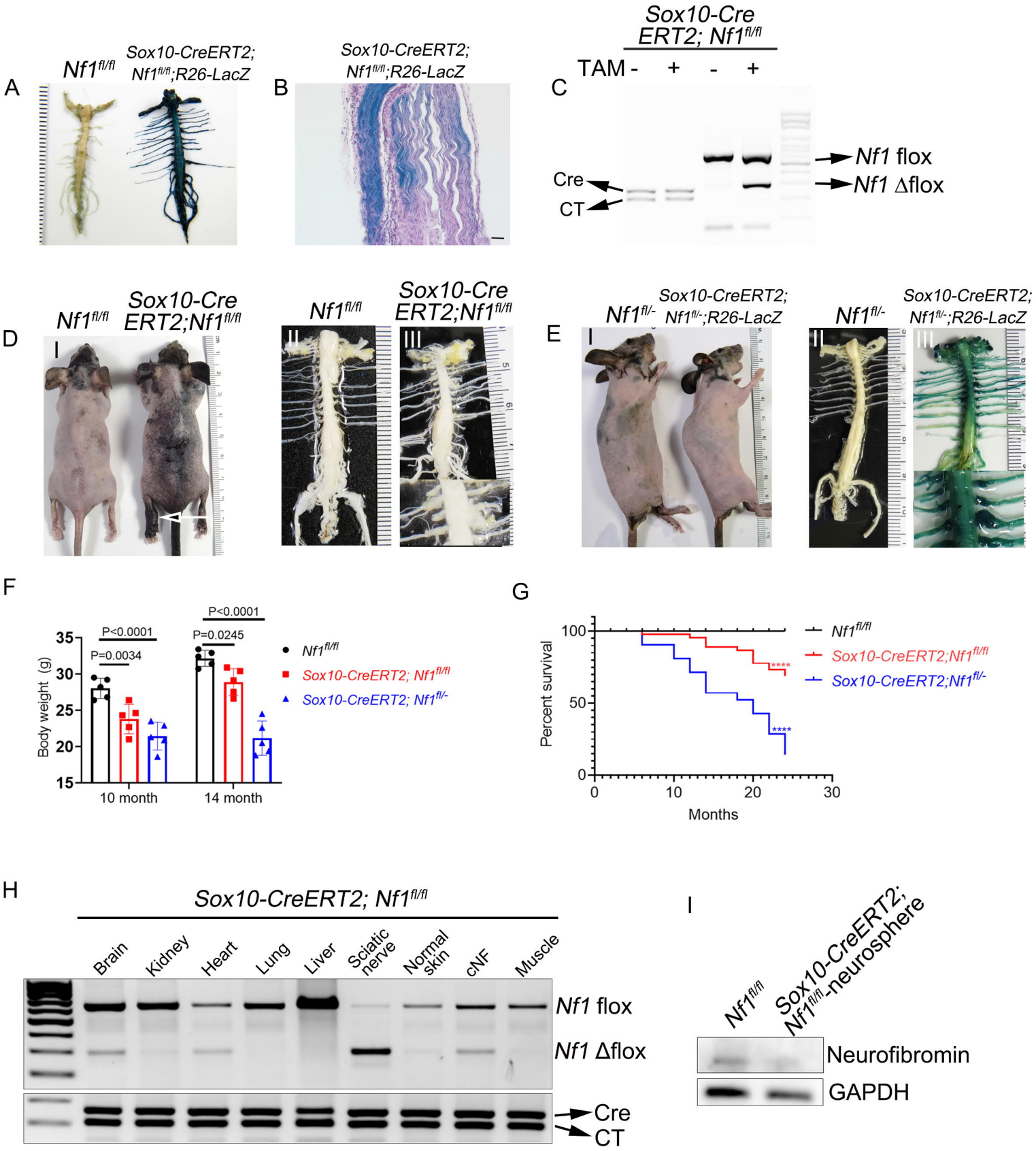

Supplemental Figure 5. Characterization of *Sox10-CreERT2; Nf1$^{fl/fl}$* mice (related to Figure 7). (A-B) After tamoxifen treatment, LacZ was expressed in the spinal cord (**A**) and sciatic nerve (**B**). **(C)** *Nf1* deletion between two LoxP sites in *Sox10-CreERT2; Nf1$^{fl/fl}$* mice after tamoxifen administration was confirmed by demonstration of a Δflox band. **(D)** A representative *Sox10-CreERT2; Nf1$^{fl/fl}$* mouse with a classic giant diffuse plexiform neurofibroma (arrow) after tamoxifen treatment exhibits a giant thigh/leg tumor and enlarged DRGs (Insert in III). This representative plexiform neurofibroma on thigh/leg in D-I was from the same mouse that is shown in Figure 7B. **(E)** A representative *Sox10-CreERT2; Nf1$^{fl/-}$; R26-LacZ* mouse with a pNF showed spinal cord curve kyphosis and enlarged DRGs (Insert in III). Scale bar, 50 μm. **(F)** Comparison of body weights between *Nf1$^{fl/fl}$*, *Sox10-CreERT2; Nf1$^{fl/fl}$* and *Sox10-CreERT2; Nf1$^{fl/-}$* mice. Comparisons among groups were performed by one-way ANOVA. **(G)** Kaplan-Meier survival curves of *Nf1$^{fl/fl}$*, *Sox10-CreERT2; Nf1$^{fl/fl}$* and *Sox10-CreERT2; Nf1$^{fl/-}$* mice with log-rank statistical test. **(H)** Genomic DNA was isolated from different tissues in *Sox10-CreERT2; Nf1$^{fl/fl}$* mice and genotyping for *Nf1* flox and *Nf1* Δflox was measured by PCR. **(I)** Neurofibromin expression in neurospheres isolated from cNFs of *Sox10-CreERT2; Nf1$^{fl/fl}$* mice was determined by western blot. GAPDH was the loading control.

Supplemental Figure 6

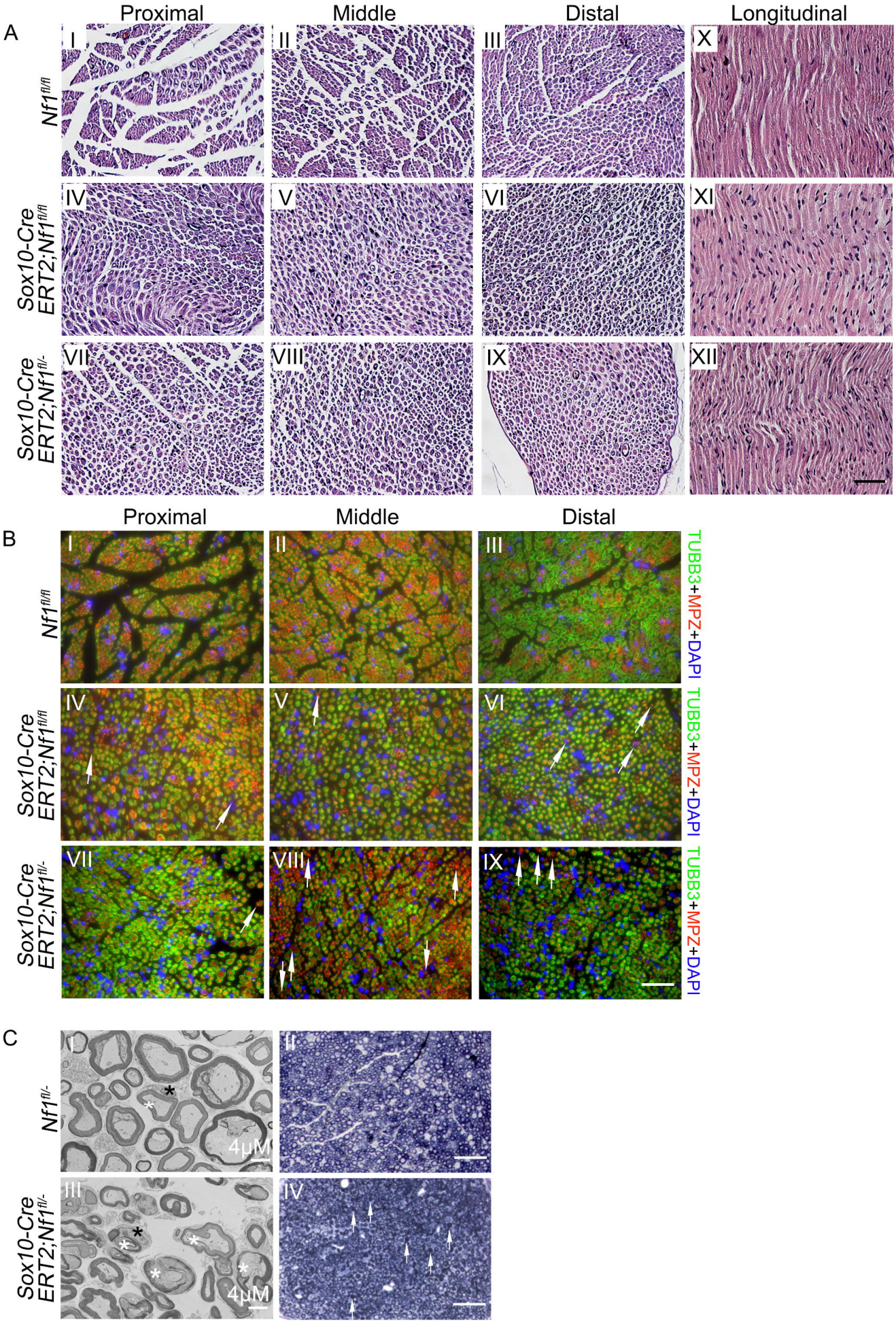

Supplemental Figure 6. *Nf1* loss in SOX10-expressing cells impairs Schwann cell lineage differentiation *in vivo* (related to Figure 7). (A) Sciatic nerves from *Nf1$^{fl/fl}$, Sox10-CreERT2; Nf1$^{fl/fl}$ and Sox10-CreERT2; Nf1$^{fl/-}$* mice were cross-sectioned (I to IX) and longitudinally sectioned (X to XII). H&E showed that mutant sciatic nerves lost the nerve bundles with fascicular organization compared to controls (I to IX). Mutant sciatic nerves were more hypercellular than controls (X to XII). n = 3. **(B)** Mutant sciatic nerves developed more non-myelinated axons (white arrows) compared to controls. n = 3. **(C)** Electron micrographs (I and III) showed that mutant sciatic nerves had non-myelinated and immature sheath surrounding the axon (white star in III). Black star shows a Schwann cell surrounding an axon. Toluidine blue staining (II and IV) showed the increased numbers of cells between myelinated axons in the mutant sciatic nerves (white arrows in IV). Scale bar, 50 μm unless otherwise noted.

Supplemental Figure 7

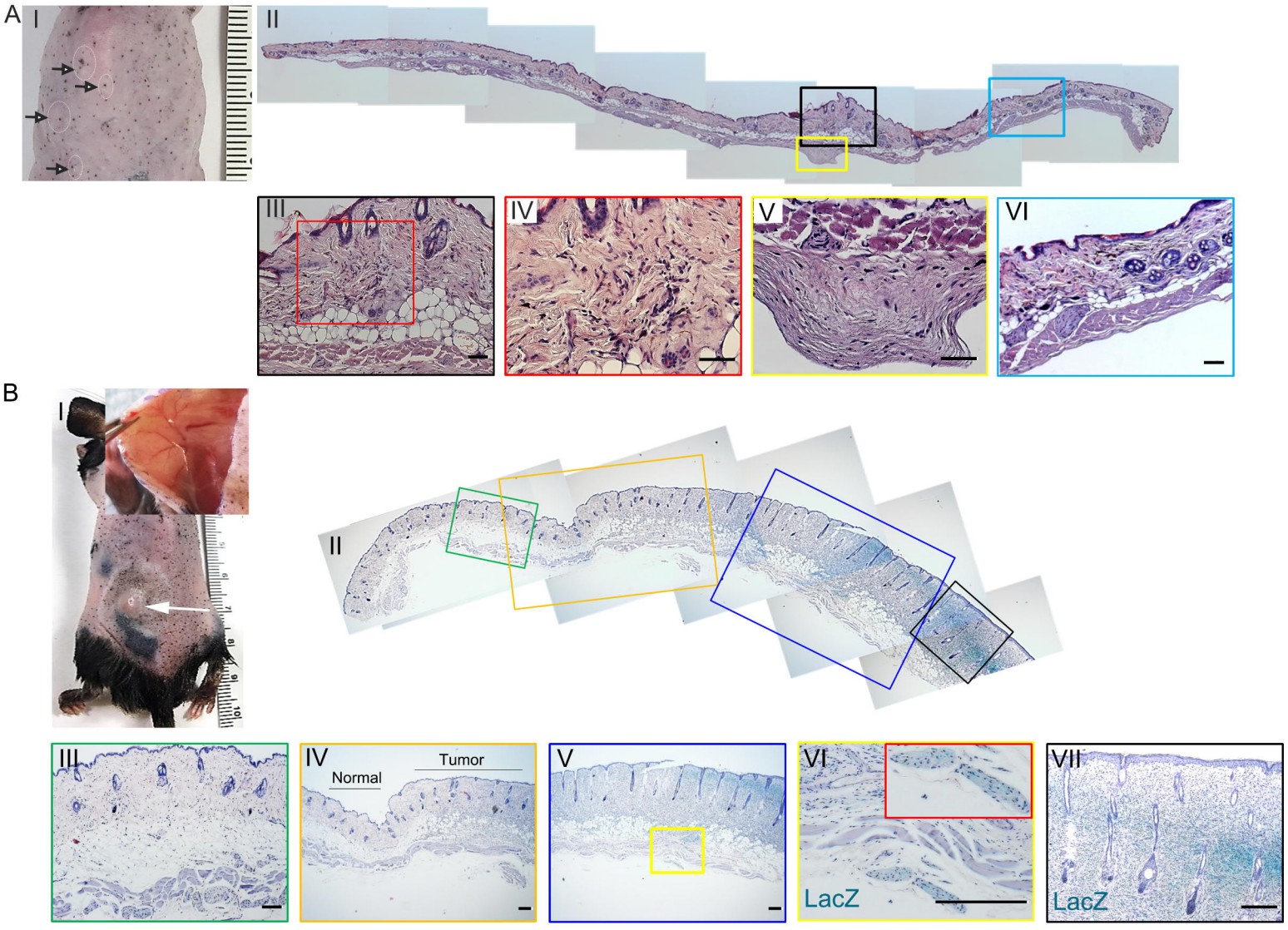

Supplemental Figure 7. SOX10-expressing cells contain the cNF tumor-initiating cells (related to Figure 8). (A) *Sox10-CreERT2; Nf1$^{fl/fl}$; R26-LacZ* mice developed early signs of discrete cutaneous neurofibromas (circles in I and squares in II) following tamoxifen treatment, showing hypercellularity (III and IV) and enlarged nerves (V) compared to the "normal" skin distant from the tumor (VI). **(B)** Upon tamoxifen treatment, *Sox10-CreERT2; Nf1$^{fl/fl}$; R26-LacZ* mice gradually developed discrete cutaneous neurofibromas (I), with a distinct transition from thin skin to thick skin (II - V). The tumor area had accumulation of nerves (VI) and LacZ-positive SOX10 lineage cells (VII). These representative mouse skin pictures with cutaneous neurofibroma in B-I were from the same mouse that is shown in Figure 8A. Scale bar, 50 μm.

Supplemental Figure 8

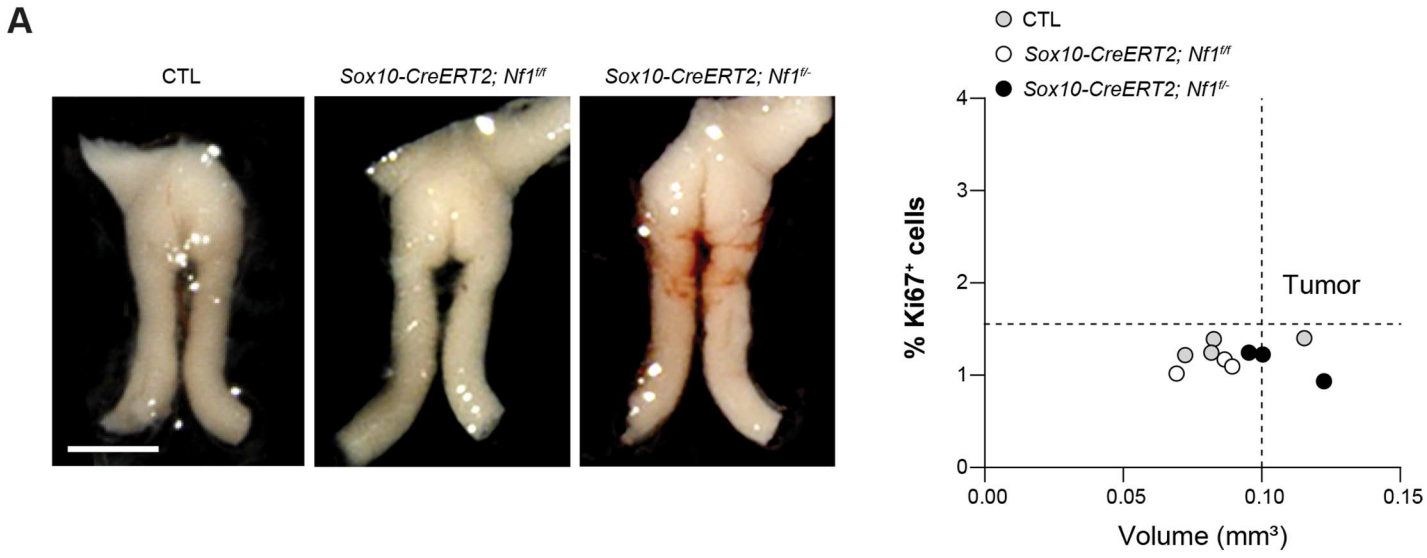

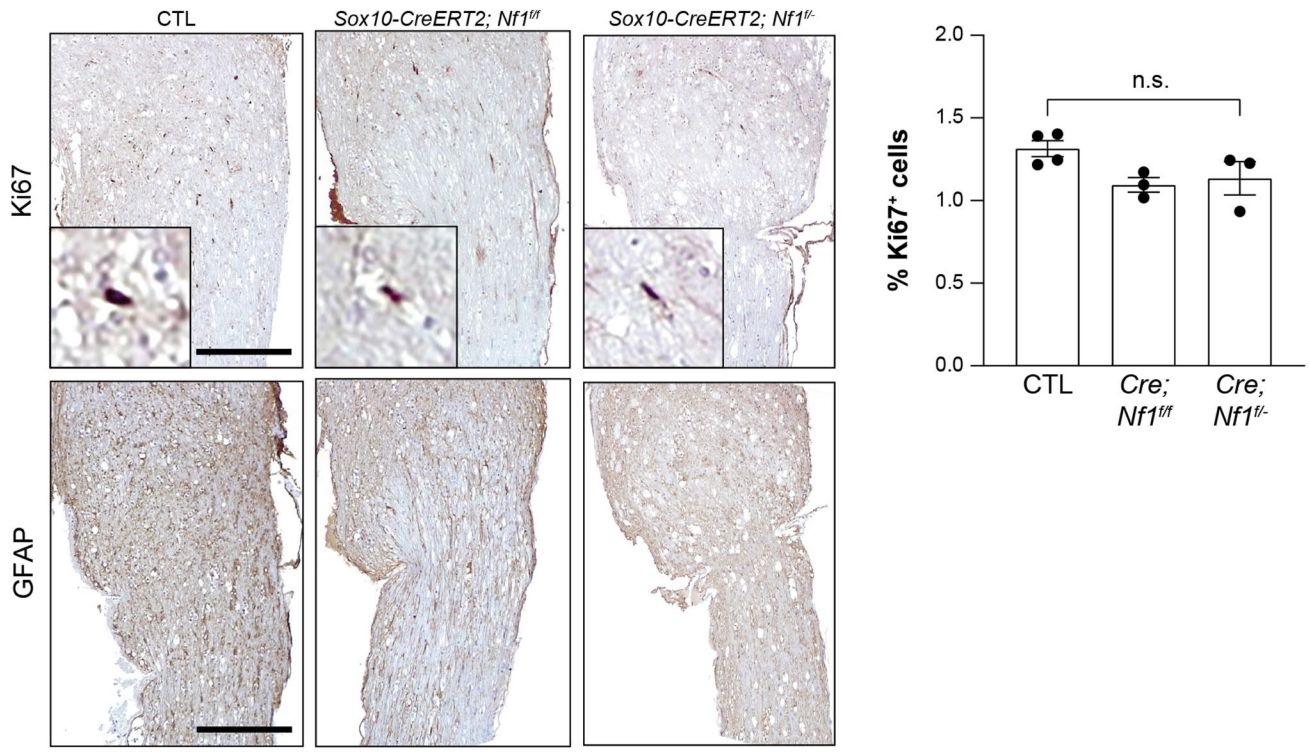

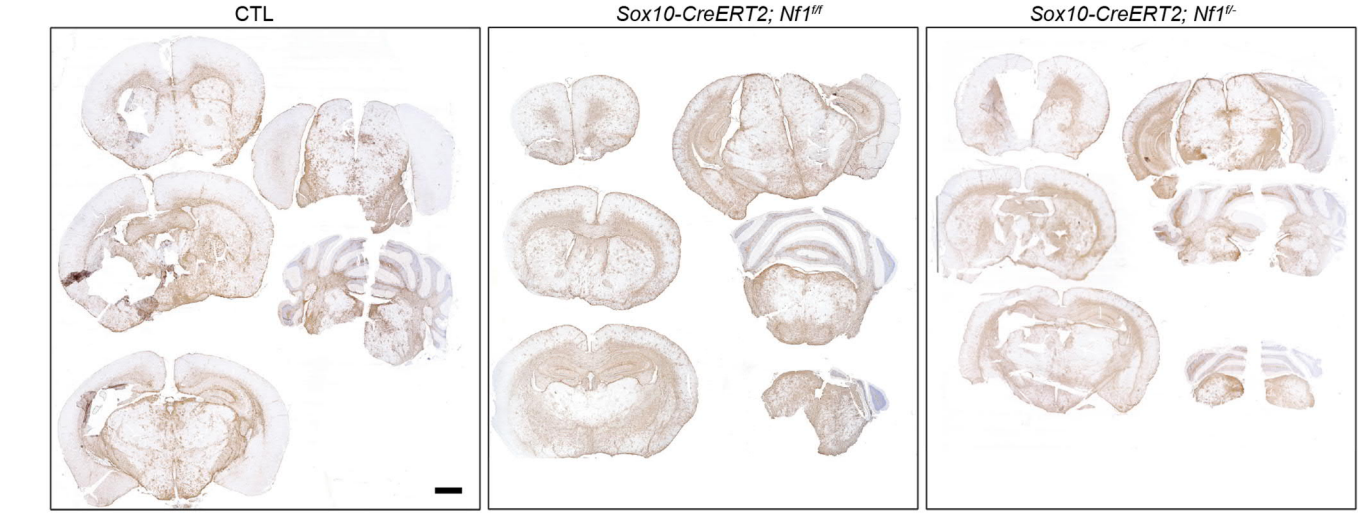

Supplemental Figure 8. *Sox10*-CreERT; *Nf1*$^{fl/-}$ mice do not develop central nervous system tumors. (A) Representative gross images of optic nerves (left panel) from *Sox10-CreERT; Nf1*$^{fl/-}$ mice and *Sox10-CreERT; Nf1*$^{fl/fl}$ mice, compared to *Nf1*$^{fl/fl}$ controls (CTL), with prechiasmatic optic nerve volumes plotted against their respective percentage of Ki67^{+} cells (rig*ht panel*). Scale bar, 1 mm. (**B)** Representative Ki67 and GFAP immunostaining of *Sox10-Cre; Nf1*$^{fl/fl}$ and *Sox10-Cre; Nf1*$^{fl/-}$ optic nerves, compared to *Nf1*$^{fl/fl}$ controls**.** Quantitation of the percent of Ki67^{+} cells is shown in the graph (right). Data are presented as the mean ± SEM. One-way ANOVA with Bonferroni post-test correction. n.s., not significant. Scale bar, 100 μm. **(C)** Representative GFAP-immunostained whole brain sections from *Sox10-Cre; Nf1*$^{fl/fl}$ and *Sox10-Cre; Nf1*$^{fl/-}$ mice compared to *Nf1*$^{fl/fl}$ controls**.** No optic gliomas or brain tumors were identified in any of the mutant mice. Scale bar, 100 μm.

Supplemental Table 1. Band intensity ratios (related to Figures 2)

Cell line	p-ERK/ t-ERK	p-ERK/ GAPDH	t-ERK/ GAPDH	GAP43/ GAPDH	SOX10/ GAPDH	p53/ GAPDH	
NF1+/- hiPSCs-SCPs	0.37	0.30	0.79	1.07	0.82	0.99	
NF1-/- hiPSCs-SCPs	0.49	0.60	1.23	1.47	0.69	0.77	
	p-ERK/ t-ERK	**p-ERK/ GAPDH**	**t-ERK/ GAPDH**	**GAP43/ GAPDH**	**SOX10/ GAPDH**	**p53/ GAPDH**	**Nestin/ GAPDH**
$Nf1^{fl/fl}$-GFP	0.95	0.19	0.20	0.54	0.31	0.23	0.20
$Nf1^{fl/fl}$ -Cre	0.68	0.28	0.41	0.69	0.24	0.21	0.28

Supplemental Table 2. Resources/Chemicals used

Name	Company	Catalog No.
DMEM/F12	Gibco	Cat#12-634-028
Neurobasal medium	Gibco	Cat#21103049
N2	Gibco	Cat#17502-048
B27	Gibco	Cat#12587-010
mTeSR plus medium	STEMCELL Technologies	Cat#5825
StemPro™ Accutase™ Cell Dissociation Reagent	Thermofisher	Cat#A1110501
ROCK inhibitor (Y-27632)	STEMCELL Technologies	Cat#72304
Cryostor CS10	STEMCELL Technologies	Cat#07930
Probumin BSA	EMD Millipore	Cat# 810683
Glutamax	Gibco	Cat#35050-061
Non-essential amino acid	Corning	Cat#25-025-CI
Trace A	Corning	Cat#25-021-CI
Trace B	Corning	Cat#25-022-CI
Trace C	Corning	Cat#25-023-CI
Bovine transferrin	Invitrogen	Cat#11107-018
(+)-sodium l-ascorbate	Sigma	Cat# A4034
LONGR3 IGF-I	Sigma	Cat#85580C
CHIR99021	STEMCELL Technologies	Cat# 72052
Human recombinant FGF2	Thermo Fisher	Cat#PHG0360
Neuregulin β-1	Peprotech	Cat#AF-100-03
SB431542	EMD Millipore	Cat#61-6461-5MG
Y27632 (ROCK inhibitor)	STEMCELL Technologies	Cat#72304
LDN193189	Tocris	Cat# 60-531-0
2-mercaptoethanol	Gibco	Cat#21985-023
L-15 medium	Sigma	Cat#L1518
pMD2.G	Addgene	Plasmid#12259
psPAX2	Addgene	Plasmid#12260
LentiCRISPRv2	Addgene	Plasmid#52961
Ad5CMVGFP	University of Iowa	VVC-U of Iowa-4
Ad5CMVCre-eGFP	University of Iowa	VVC-U of Iowa-1174-HT
iTaq™ Universal SYBR Green Supermix	BIO-RAD	Cat#172-5124
iScript™ Select cDNA Synthesis Kit	BIO-RAD	Cat#1708897
2XTaq RED Master Mix	Apex	Cat#5200300-1250

NucleoBond Xtra Midi	Macherey-Nagel	Cat#740410.100
PD0325901	Selleckchem	Cat#S1036

Supplemental Table 3. Antibodies used

Antibody	Company	Identifier
Mouse monoclonal anti NGFR (p75)	Advanced Targeting Systems	Cat#AB-N07, RRID: AB_171797
Chicken polyclonal anti GAP43	Novus	Cat#NBP1-92714, RRID: AB_11023277
Rabbit polyclonal anti S100β	Agilent	Cat# Z0311 RRID: AB_10013383
Rabbit polyclonal anti GAP43	Abcam	Cat#ab12274, RRID: AB_2247459
Mouse monoclonal anti SOX10 (A-2)	Santa Cruz	Cat#sc-365692, RRID: AB_2721184
Rabbit monoclonal anti SOX10 [EPR4007-104]	Abcam	Cat#ab180862, RRID: AB_2721184
Chicken polyclonal anti nestin	Abcam	Cat#ab134017, RRID: AB_2753197
Rabbit polyclonal anti phospho-H3 (Ser10)	Cell Signaling	Cat#9701, RRID: AB_331535
Rabbit monoclonal anti phospho-ERK1/2	Cell Signaling	Cat#4370, RRID: AB_2315112
Rabbit monoclonal anti total ERK1/2	Cell Signaling	Cat#4695, RRID: AB_390779
Rabbit monoclonal anti phospho-s6	Cell Signaling	Cat#4858 RRID: AB_916156
Rabbit monoclonal anti total s6	Cell Signaling	Cat#2217 RRID: AB_331355
Rabbit polyclonal anti Iba1	Wako	Cat#019-19741 RRID: AB_839504
Rabbit monoclonal anti Ku80	Cell signaling	Cat#2180, RRID: AB_2218736
Mouse monoclonal anti Cas9 (7A9-3A3)	Santa Cruz	Cat#sc-517386, RRID: AB_2800509
Goat polyclonal anti Oct3/4 (N-19)	Santa Cruz	Cat#sc-8628, RRID: AB_653551
Mouse monoclonal anti Oct3/4 (C-10)	Santa Cruz	Cat#sc-5279, RRID: AB_628051
Mouse monoclonal anti TRA1-60	Invitrogen	Cat#41-1000, RRID: AB_2533494
Rabbit polyclonal anti NANOG (N3C3)	GeneTex	Cat#GTX100863, RRID: AB_10615506
Mouse monoclonal anti SOX2	R&D	Cat#MAB2018, RRID: AB_358009
Mouse monoclonal anti HNK1 (CD57)	Sigma	Cat#C6680-50TST, RRID: AB_1078474
Mouse monoclonal anti AP2-alpha	DSHB	Cat#3B5, RRID: AB_528084
Mouse monoclonal anti GAPDH (6c5)	Santa Cruz	Cat#sc-32233, RRID: AB_627679

Rabbit monoclonal anti p53 [26]	Abcam	Cat#ab32389, RRID: AB_776981
Mouse monoclonal anti APC-p75 IgG1 (clone 74902)	R&D	Cat#FAB367A RRID: AB_10920942
Mouse monoclonal anti APC-isotype IgG1 (clone 11711)	R&D	Cat#IC002A RRID: AB_357239
Rabbit polyclonal anti neurofibromin	Santa Cruz	Cat#sc-67, RRID: AB_2149681
Rabbit polyclonal anti HOXb7	Novus	Cat#NBP2-14098, RRID: AB_2721144

Supplemental Table 4. qPCR primers used (related to Figures 2 and 5)

Gene Symbol	Primer Sequence (5'-3')	NCBI RefSeq	Species
actin beta	F: ACCTTCTACAATGAGCTGCG R: CCTGGATAGCAACGTACATGG	NM_001101.3	*Homo sapiens*
CDH19	F: ACAAGCGTCTGTAACTCTGGG R: AGCAAACTTCGTGTTGGACA	NM_021153.4	*Homo sapiens*
ErbB3	F: GGTGCTGGGCTTGCTTTT R: CGTGGCTGGAGTTGGTGTTA	NM_001982	*Homo sapiens*
GAP43	F: AGCCAAGCTGAAGAGAACATAG R: TCAGGCATGTTCTTGGTCAG	NM_002045	*Homo sapiens*
HOXB7	F: CCTGGATGCGAAGCTCAG R: CGTCAGGTAGCGATTGTAGTG	NM_004502.4	*Homo sapiens*
ITGA4	F: AGCCCTAATGGAGAACCTTGT R: CCAGTGGGGAGCTTATTTTCAT	NM_000885.6	*Homo sapiens*
MPZ	F: AAGTGCCAACTAGGTACGGG R: CATAGCACTGAGCCTCCTCT	NM_001315491.1	*Homo sapiens*
nestin	F: CAGCGTTGGAACAGAGGTTA R: GCTGGCACAGGTGTCTCAAG	NM_006617.1	*Homo sapiens*
PAX3	F: GTTTCGCCTTCACCTGGATA R: GTTGATAAAAACACCGCCGA	NM_000438	*Homo sapiens*
PLP1	F: CAGTCTATTGCCTTCCCCAG R: CAGATGGACAGAAGGTTGGAG	NM_000533.5	*Homo sapiens*
p21	F: CATGTGGACCTGTCACTGTCTTGTA R: GAAGATCAGCCGGCGTTTG	NM_001374511.1	*Homo sapiens*
p75NTR	F: CGGCACGTATTCCGACG R: GGTGTGGACCGTGTAATCC	NM_002507.4	*Homo sapiens*
SLUG	F: CGAACTGGACACACATACAGTG R: CTGAGGATCTCTGGTTGTGGT	NM_003068.5	*Homo sapiens*
SNAI1 (SNAIL)	F: TCCACGAGGTGTGACTAACTATGC R: GAATAGTTCTGGGAGACACATCGG	NM_005985.4	*Homo sapiens*
SOX2	F: GCTGCAAAAGAGAACACCAATCCC R: AAACTTCCTGCAAAGCTCCTACCG	NM_003106.4	*Homo sapiens*
SOX10	F: CCTCACAGATCGCCTACACC R: CATATAGGAGAAGGCCGAGTAGA	NM_006941.4	*Homo sapiens*
TP53	F: GCCCAACAACACCAGCTCCT R: GCCCAACAACACCAGCTCCT	NM_001126114.2	*Homo sapiens*
TWIST1	F: GTCCGCAGTCTTACGAGGAG R: GCTTGAGGGTCTGAATCTTGCT	NM_000474.4	*Homo sapiens*

actin beta	F: CCTCTATGCCAACACAGT R: AGCCACCAATCCACACAG	NM_007393.5	*Mus musculus*
Bmi1	F: CTGGAGAAGAAATGGCCCACTA R: CTCATCTTCATTCTTTTGCAAGTTG	NM_007552.4	*Mus musculus*
Ccnd2	F: ACCTCCCGCAGTGTTCCTATTTCA R: AGTCAGCGGGATGGTCTCTTTCAG	NM_009829.3	*Mus musculus*
c-jun	F: CTGAGTGTGCGAGAGACAGC R: CCAAGTCCGTCCGTCTGT	NM_010591.2	*Mus musculus*
Cd133 (prominin-1)	F: GAAGGAGCCCAGCTTAGAGG R: GGTCATTCACTCAAAGTACCATCC	NM_001163577.1	*Mus musculus*
Dhh	F: CATGTGGCCCGGAGTACGCC R: CGCTGCATCAGCGGCCAGTA	NM_007857.5	*Mus musculus*
ErbB3	F: GAGCGGGGTGACGGGAGTAA R: GGGTCGCGAACAGTTCTCCC	NM_010153.2	*Mus musculus*
Ednrb	F: TCAGAAAACAGCCTTCATGC R: GCGGCAAGCAGAAGTAGAAA	NM_001136061.2	*Mus musculus*
Gap43	F: AAGGCAGGGGAAGATACCAC R: TTGTTCAATCTTTTGGTCCTCAT	NM_008083.2	*Mus musculus*
Hey2	F: GTGGGGAGCGAGAACAATTA R: GTTGTCGGTGAATTGGACCT	NM_013904.1	*Mus musculus*
Hmga2	F: AAGGCAGCAAAAACAAGAGC R: CCGTTTTTCTCCAATGGTCT	NM_001347170.1	*Mus musculus*
Hopx	F: CGGAGGACCAGGTGGAGAT R: CCGGGTGCTTGTTGACCTT	NM_001159900.1	*Mus musculus*
Id2	F: GACAGAACCAGGCGTCCA R: AGCTCAGAAGGGAATTCAGATG	NM_010496.3	*Mus musculus*
Igf2bp2	F: GGGAAAATCATGGAAGTTGACTA R: CGGGATGTTCCGAATCTG	NM_183029.2	*Mus musculus*
Krox20 (Egr2)	F: AATGGCTTGGGACTGACTTG R: GCCAGAGAAACCTCCATTCA	NM_010118.3	*Mus musculus*
Krt42	F: AGGAGCTGGCCTATCTGAGG R: GGCGTCCATCTCCACATT	NM_212483.3	*Mus musculus*
Lif	F: AATGCCACCTGTGCCATACG R: CAACTTGGTCTTCTCTGTCCCG	NM_008501.2	*Mus musculus*
Lgr5	F: CAGTGTGGACGACCTTCATAAGAA R: AAGGTCCCGCTCATCTTGAAC	NM_010195.2	*Mus musculus*
Mgll	F: GCAGTGGAACATCTCAACCA R: AGGGAGGCTGTTCCCCTAT	NM_001166251.1	*Mus musculus*
Olfm4	F: TGGCCCTTGGAAGCTGTAGT R: ACCTCCTTGGCCATAGCGAA	NM_001351947.1	*Mus musculus*
p75NTR	F: GGTGATGGCAACCTCTACAGT R: CCTCGTGGGTAAAGGAGTCTA	NM_033217.3	*Mus musculus*
S100β	F: GACTCCAGCAGCAAAGGTGAC R: CATCTTCGTCCAGCGTCTCCA	NM_009115.3	*Mus musculus*
Slug	F: CTGCGGCAAGGCGTTT R: CGTGTGAGTTCTAATGTGTCCTTGA	NM_001168276.1	*Mus musculus*
Sox2	F: GCTGGACTGCGAACTGGA R: GCGTTAATTTGGATGGGATTG	NM_011443.4	*Mus musculus*
Sox10	F: CAGGTGTGGCTCTGCCCACG R: GTGTAGAGGGGCCGCTGGGA	NM_011437.1	*Mus musculus*

Supplemental Table 5. Primers used for CRISPR-Cas9 plasmid (related to Figure 5)

Name	Primer sequence (5'-3')	PAM	NCBI RefSeq
sgTP53-1	F: CACCGGCATGGGCGGCATGAACCGG R: AAACCCGGTTCATGCCGCCCATGCC	GCATGGGCGGCAT GAACCGGAGG	NM_001126114.2
sgTP53-2	F: CACCGCCCCTTGCCGTCCCAAGCAA R: AAACTTGCTTGGGACGGCAAGGGGC	CCCCTTGCCGTCC CAAGCAATGG	NM_001126114.2
sgTP53-3	F: CACCGGGGCAGCTACGGTTTCCGTC R: AAACGACGGAAACCGTAGCTGCCCC	GGGCAGCTACGGT TTCCGTCTGG	NM_001126114.2
sgTP53-4	F: CACCGGGCAGCTACGGTTTCCGTCT R: AAACAGACGGAAACCGTAGCTGCCC	GGCAGCTACGGTT TCCGTCTGGG	NM_001126114.2
LentiCRISPRv2-Screen	F: GTACCGAGGGCCTATTTCCC R: CTCCTTTCAAGACCTAGCTAGCG		

Supplemental Table 6. Genotyping primers (related to Figures 7 and 8)

Mouse strain	Cre	Internal control
Sox10-Cre	F: CACCTAGGGTCTGGCATGTG R: AGGCAAATTTTGGTGTACGG	F: GACAAAATGGTGAAGGTCGG R: CAAAGGCGGAGTTACCAGAG
Sox10-CreERT2	F: CACCTAGGGTCTGGCATGT R: CAGGTTTTGGTGCACAGTCA	F: CAAATGTTGCTTGTCTGGTG R: GTCAGTCGAGTGCACAGTTT
Nf1 flox	AATGTGAAATTGGTGTCGAGTAAGGTAACCAC	
	TTAAGAGCATCTGCTGCTCTTAGAGGGAA	
	TCAGACTGATTGTTGTACCTGATGGTTGTACC	
LacZ	F: ATTGTCAGACATGTATACCCCGTACGTCTT R: TTTTGACACCAGACCAACTGGTAATGGTAG	

Supplemental Table 7. List of SOX10-CreERT2 mice (related to Figure 7 and 8)

Genotype	Sex	pNF	cNF	Life span (days)
Sox10-CreERT2; Nf1$^{f/f}$	M	Y	Y	575
Sox10-CreERT2; Nf1$^{f/f}$	M	Y	Y	518
Sox10-CreERT2; Nf1$^{f/f}$	F	Y	Y	471
Sox10-CreERT2; Nf1$^{f/f}$	M	Y	Y	488
Sox10-CreERT2; Nf1$^{f/f}$	F	Y	Y	403
Sox10-CreERT2; Nf1$^{f/f}$	F	N	Y	548
Sox10-CreERT2; Nf1$^{f/f}$	M	Y	Y	509
Sox10-CreERT2; Nf1$^{f/f}$	F	Y	Y	457
Sox10-CreERT2; Nf1$^{f/f}$	M	Y	Y	489
Sox10-CreERT2; Nf1$^{f/f}$	F	Y	Y	546
Sox10-CreERT2; Nf1$^{f/f}$	M	Y	Y	214
Sox10-CreERT2; Nf1$^{f/f}$	F	Y	Y	392
Sox10-CreERT2; Nf1$^{f/f}$	M	Y	Y	495
Sox10-CreERT2; Nf1$^{f/f}$	M	Y	Y	411
Sox10-CreERT2; Nf1$^{f/f}$	M	Y	Y	560

Sox10-CreERT2; Nf1$^{f/f}$	M	Y	N	247
Sox10-CreERT2; Nf1$^{f/f}$	M	Y	Y	247
Sox10-CreERT2; Nf1$^{f/f}$	M	Y	Y	335
Sox10-CreERT2; Nf1$^{f/f}$	F	Y	Y	470
Sox10-CreERT2; Nf1$^{f/f}$	F	Y	Y	470
Sox10-CreERT2; Nf1$^{f/f}$	M	Y	Y	401
Sox10-CreERT2; Nf1$^{f/f}$	F	Y	Y	326
Sox10-CreERT2; Nf1$^{f/f}$	F	Y	Y	412
Sox10-CreERT2; Nf1$^{f/f}$	F	Y	Y	548
Sox10-CreERT2; Nf1$^{f/f}$	M	Y	Y	350
Sox10-CreERT2; Nf1$^{f/-}$	F	Y	Y	451
Sox10-CreERT2; Nf1$^{f/-}$	F	Y	Y	411
Sox10-CreERT2; Nf1$^{f/-}$	F	Y	N	199
Sox10-CreERT2; Nf1$^{f/-}$	M	Y	N	205
Sox10-CreERT2; Nf1$^{f/-}$	F	Y	Y	263
Sox10-CreERT2; Nf1$^{f/-}$	M	Y	Y	304
Sox10-CreERT2; Nf1$^{f/-}$	F	Y	Y	304
Sox10-CreERT2; Nf1$^{f/-}$	F	Y	N	190
Sox10-CreERT2; Nf1$^{f/-}$	F	Y	Y	475
Sox10-CreERT2; Nf1$^{f/-}$	M	Y	Y	190
Sox10-CreERT2; Nf1$^{f/-}$	M	Y	N	314
Sox10-CreERT2; Nf1$^{f/-}$	M	Y	Y	418
Sox10-CreERT2; Nf1$^{f/-}$	F	Y	Y	418
Sox10-CreERT2; Nf1$^{f/-}$	F	Y	Y	418
Sox10-CreERT2; Nf1$^{f/-}$	M	Y	N	399
Sox10-CreERT2; Nf1$^{f/-}$	F	Y	Y	420
Sox10-CreERT2; Nf1$^{f/-}$	F	Y	Y	337
Sox10-CreERT2; Nf1$^{f/-}$	F	Y	Y	200
Sox10-CreERT2; Nf1$^{f/-}$	F	Y	Y	184

F: female; M: male; Y: yes; N: no.